POLITECNICO DI TORINO

Dipartimento di Ingegneria Meccanica e Aerospaziale

Corso di Laurea Magistrale in Ingegneria Meccanica

Tesi di laurea

Traction Control System development for an AWD hybrid vehicle

Relatori:
Prof. Alessandro Vigliani
Ing. Antonio Tota

Tutor aziendale:
Ing. Salvatore Calanna

Candidata:
Roberta Laneve

Dicembre 2020

Contents

List of figures

List of tables

Acknowledgments

Desidero ringraziare il Politecnico di Torino e Danisi Engineering per avermi dato l'opportunità di partecipare ad un interessante progetto, in un anno sicuramente non poco complesso.

Ringrazio i miei relatori prof. Alessandro Vigliani e ing. Antonio Tota, per i preziosi suggerimenti e le conoscenze trasmesse.

Grazie al gruppo AVD di Danisi Engineering per avermi accolta in questi mesi, ed in particolare il mio tutor ing. Salvatore Calanna per avermi guidata con dedizione e professionalità in questo percorso.

Abstract

The purpose of this thesis work is to design a Traction Control System algorithm for an All-Wheel-Drive (AWD) hybrid vehicle. Generally, the control aim is to prevent the driven wheels from spinning in order to guarantee vehicle stability, especially on slippery roads. In this specific case, the control logic has to be also adapted for three vehicle driving modes: *Comfort*, *Wet,* and *Sport*. The work is developed in collaboration with *Danisi Engineering* company (Nichelino – TO).

First of all, the 14-degrees-of-freedom vehicle model is implemented on the *VI-CarRealTime* software, and its overall dynamic performances are evaluated. The vehicle object of this study is a high-performance one, equipped with two independent electric motors on front wheels and an internal combustion engine on rear axle.

The control structure is developed on *MATLAB-Simulink* environment: starting from setting general control aims, the differences among the three driving modes are established. The controller acts on the vehicle powertrain, reducing motors and engine output torques in case of wheels excessive rotation. Proportional-Integral (PI) controllers are adopted for torques regulation.

The three Traction Control modes performances are at first assessed through off-line tests, which consist of co-simulations of *VI-CarRealTime* and *MATLAB-Simulink* environments. The passive and the controlled vehicles are compared on different scenarios to verify the effectiveness of control action: a straight-line maximum acceleration manoeuvre is performed on different road conditions, including constant mu-split, variable mu-split and low friction surfaces. The same set of scenarios is also used to analyse the differences between the proposed control and an internal *VI-CarRealTime* one. Tests' results show how all the designed control achieves its task, enhancing vehicle stability and acceleration performance. Finally, on-line acceleration manoeuvres tests are performed: vehicle model and control are implemented on a dynamic driving simulator. During tests executions the driver's subjective feedback is collected, to evaluate how the control activation affects driver perception of the vehicle dynamic behaviour.

1 Introduction

In recent decades, vehicle safety and comfort have gathered increasing interest in the automotive field. For this purpose, over the past years active safety technologies have been developed and improved: they are systems that actively intervene in vehicle operations, generally limiting the movement and retarding the vehicle itself, in order to stabilize its handling response in critical situations and maintain its steerability. These systems aim to support the driver in difficult driving conditions preventing accidents and, thus, contributing to road safety [1]. Among them, Traction Control System (TCS), also called Anti Slip Regulation (ASR), plays an important role: it enhances vehicle's longitudinal performances preventing the driving wheels from spinning when the vehicle accelerates excessively, particularly on low friction roads and during cornering. In fact, the loss of traction of wheels leads not only to reduced vehicle velocity or acceleration in the longitudinal direction, but also, due to tire behaviour, to a poor lateral performance, so it compromises vehicle handling and stability and it does not react in the way that the driver would generally expect [1]. In this context, it is clear that TCS action is fundamental; therefore, it started to be implemented during the 1990s, initially as an expansion of ABS (TCS can be considered the counterpart of ABS substantially), and nowadays it is widespread in all the vehicles [2].

Nowadays, new development and improvement of TCS algorithms can be achieved with vehicles powered, partially or totally, by electric motors: with Emissions Standards requiring even more significant reductions in vehicle emissions, automotive constructors show a recent interest in powertrain electrification. Hybrid Electric Vehicles (HEV) seem to be the most successful solution, representing the best compromise between high performances demand and fuel efficiency: the presence of conventional Internal Combustion Engine (ICE) permits to overcome the autonomy range limits of batteries, which affect pure Electric Vehicles, and at the same time the electric powertrain allows better management of engine functioning, optimizing its operation [3][4]. An HEV

powertrain can be defined as *parallel* or *series*: in the first case, both engine and electric motors power can be used for propulsion because each of them is connected to the wheels independently; in the other case, the engine charges the electric motors' batteries through a generator, thus it has no direct connection to vehicle wheels [3].

The presence of a hybrid electric powertrain architecture, both parallel and series, influences TCS design: the controller regulates wheels' longitudinal slips mainly acting on the wheel driving torque, which is reduced in case of excessive wheels rotation; torque limiting is achieved acting on different parameters for ICEs and electric motors.

For vehicles driven by conventional ICEs, TCS usually reduces engine torque through various methods: regulating the air amount through throttle valve opening, reducing the injected fuel quantity, modifying the ignition timing, cutting spark ignition. In addition, TCS can limit the slip also adding a braking torque contribute, so increasing brake pressure: brake system response to control activation is faster than engine one and also permits to differentiate the control of each wheel, but using it excessively leads to a significant reduction of its lifetime; as a consequence, breaking system intervention can represent only an adjustment to the control: it is used when driving wheel slip ratio is high, for a short time, and in conjunction with engine torque regulation to avoid excessive fuel consumption [5][6]. In [7] a traction controller based only on engine torque reduction is proposed: it consists of a PID controller, integrated with a fuzzy logic controller to improve its performance. [8] shows an innovative control, including PID and ant colony optimization controller to regulate both engine torque and brake pressure.

With a hybrid powertrain, TCS can exploit the advantages of electric motors: it permits a direct torque control, which involves a fast torque response, while thermal engine control includes several delay factors; it is easy to estimate the output torque value through measuring the motor current; it is possible to control each wheel independently with the corresponding motor so that the control can be more effective in case of roads with different friction for left and

right wheels and vehicle stability and driving comfort are improved [9][10][11]. Several studies present various algorithms to control the electric powertrains. In [12] a comparison of different control strategies for electric motors is shown: the authors assess strength and weaknesses of MTTE, PID, H_∞, sliding mode controllers. [13] proposes an explicit nonlinear model predictive control method, showing the advantages with respect to a PI controller.

As regards 4WD hybrid powertrain, different solutions have been presented to combine the control of ICE and electric motors: [14] describes a PID controller improved by a fuzzy logic integration. In [4] an innovative traction control system combined with the vehicle Energy Management System is proposed: the aim of this strategy is to provide both proper vehicle traction and optimized fuel consumption. [15] shows a new sliding mode controller to achieve the maximum traction force at the wheels.

The present thesis is inserted in this scenario: this work aims to design a TCS algorithm for a four-wheel-drive Hybrid Vehicle. The vehicle object of this study is a high performance one, motorized by two independent electric motors on front wheels and an ICE on rear axle; vehicle dynamic behaviour and performances can be settled by the driver switching from *Comfort* driving mode to *Sport* or *Wet* ones. Consequently, the control logic, which is differentiated for front and rear vehicle axles, has to be adapted to achieve the task of each driving mode.

The definition of the hybrid vehicle dynamic model and the design of Traction Control System is part of a project of *Danisi Engineering* company, located in Nichelino (TO), which supported the development of the whole work sharing know-how and resources.

1.1 Thesis structure

The structure of this thesis is illustrated below:

Chapter 2: 14 DOF Vehicle dynamics. Equations of vehicle dynamics are

explained referring to a 14 DOF vehicle model: ride, handling and tire dynamics are considered. A paragraph is also dedicated to handling diagrams, which characterize vehicle behaviour.

Chapter 3: *VI–CarRealTime*. In this chapter, the implementation of the vehicle model on *VI-CarRealTime* software is shown: each vehicle subsystem is illustrated with the corresponding specifications and targets, and vehicle performances are assessed. In the last paragraph of the chapter, co-simulation with *MATLAB-Simulink* is explained: this method would be used to make the control communicate with the vehicle model.

Chapter 4: Traction Control System. The development of Traction Control logic is described: starting from explaining control aims in general, the targets expected for the three driving modes are defined. Subsequently, the control structure is illustrated, pointing out the main differences between *Comfort*, *Sport* and *Wet* mode and how they are expected to affect vehicle behaviour. Huge attention is given to the controller chosen for this purpose, which is a PID one, describing how its properties are considered suitable for Traction Control purpose. Finally, the implementation of the control algorithm on *MATLAB-Simulink* is reported.

Chapter 5: Simulation tests results. The three modes of Traction Control are tested with co-simulations between *VI-CarRealTime* and *MATLAB-Simulink* environments. Firstly, the passive vehicle and the controlled one are compared on different simulation test scenarios to assess the effectiveness of control action; three straight-line acceleration manoeuvres are taken into account, differentiated by road conditions: constant *mu-split*, variable *mu-split*, low friction. The same set of scenarios is used in the second part of the chapter to analyse the differences between the designed control and an internal *VI-CarRealTime* one.

Chapter 6: Driving Simulator results. Vehicle model and control modes are implemented on a dynamic driving simulator, in order to perform the same off-line manoeuvres tests and to obtain feedbacks by a human driver about how the control activation affects vehicle's dynamic behaviour.

2 14 DOF Vehicle dynamics

The 14 DOF vehicle model, as explained in [16], describes the dynamic behaviour in the longitudinal, lateral and vertical direction of a simplified vehicle consisting of five parts:

- the sprung mass or vehicle body, composed by 6 DOF which allow longitudinal, lateral, vertical, roll, pitch and yaw motion;
- the four unsprung masses of the wheels; each wheel has 2 DOF, consisting in vertical motion with respect to the vehicle body and its rotation around the axle.

The present model, shown in Figure 1, assumes the hypothesis of a rigid vehicle body and lumped sprung and unsprung masses.

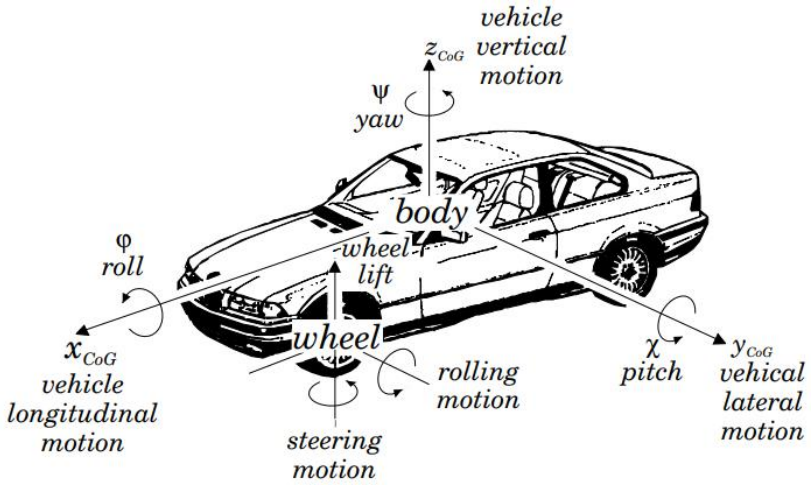

Figure 1: 14 DOF vehicle model [17]

2.1 Ride dynamics

The ride model includes 7 DOF: 3 DOF consist of vehicle body vertical displacement, roll and pitch motion, and the remaining 4 DOF consist of vertical displacement of each of four wheels. The vehicle body is connected to unsprung masses by suspensions springs and dumpers at each corner.

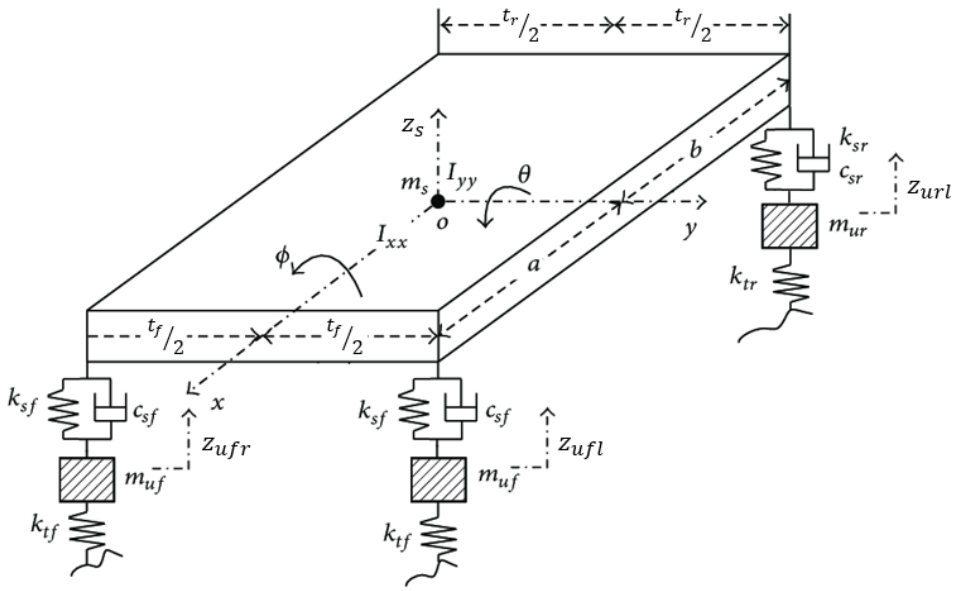

Figure 2: Vehicle ride model (adapted from [18])

According to Figure 2, it is possible to define vehicle forces equilibriums exploiting Newton second law:

- Vehicle sprung mass' vertical equilibrium:

$$F_{sfl} + F_{dfl} + F_{sfr} + F_{dfr} + F_{srl} + F_{drl} + F_{srr} + F_{drr} = m_s \ddot{z}_s \qquad (2.1)$$

  where F_{sij} and F_{dij} are respectively suspensions springs and dumpers forces for each vehicle corner; each spring is characterized by stiffness k_{si}, while each dumper is characterized by a dumping coefficient c_{si};

- Vehicle body rotational equilibrium around the y axle (pitching moment):

$$(F_{srl} + F_{drl} + F_{srr} + F_{drr})b - \big(F_{sfl} + F_{dfl} + F_{sfr} + F_{dfr}\big)a = I_p \ddot{\theta} \qquad (2.2)$$

- Vehicle body rotational equilibrium around x axle (rolling moment):

$$(F_{sfl} + F_{dfl})\frac{t_f}{2} + (F_{srl} + F_{drl})\frac{t_r}{2} - (F_{sfr} + F_{dfr})\frac{t_f}{2} - (F_{srr} + F_{drr})\frac{t_r}{2} = I_r \ddot{\phi} \qquad (2.3)$$

- Unsprung masses (wheels) vertical equilibrium:

$$\begin{cases} F_{tfl} - F_{sfl} - F_{dfl} = m_{ufl}\ddot{z}_{ufl} \\ F_{tfr} - F_{sfr} - F_{dfr} = m_{ufr}\ddot{z}_{ufr} \\ F_{trl} - F_{srl} - F_{drl} = m_{url}\ddot{z}_{url} \\ F_{trr} - F_{srr} - F_{drr} = m_{urr}\ddot{z}_{urr} \end{cases} \quad (2.4)$$

where F_{tij} are the forces due to tires stiffnesses k_{ti}.

2.2 Handling dynamics

The handling model includes 7 DOF: 3 DOF consist of vehicle body longitudinal and lateral displacement and yaw motion, and the remaining 4 DOF consist of the rotation of each wheel.

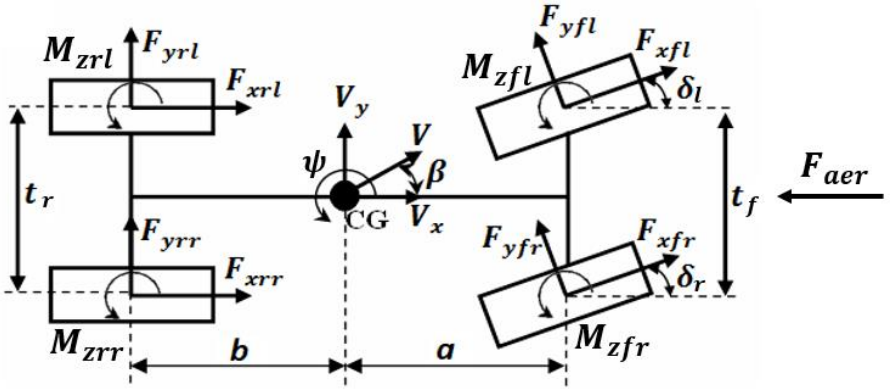

Figure 3: Vehicle handling model (adapted from [19])

In the same way of ride dynamics, vehicle forces equilibriums can be derived from Figure 3:

- Vehicle's longitudinal equilibrium:

$$F_{xfl}\cos\delta_l - F_{yfl}\sin\delta_l + F_{xfr}\cos\delta_r - F_{yfr}\sin\delta_r + F_{xrl} + F_{xrr} + \\ -\frac{1}{2}\rho C_x A_f V_x^2 \mathrm{sgn}V_x = ma_x \quad (2.5)$$

where ρ is the air density, C_x is the drag coefficient and $A_f$is the vehicle frontal area, δ_l and δ_r are respectively the left and right wheel steering angles. From (2.5), the longitudinal inertial acceleration a_x at the centre of gravity can be obtained.

- Vehicle's lateral equilibrium, through which lateral inertial CG acceleration a_y can be derived:

$$F_{xfl}\sin\delta_l + F_{yfl}\cos\delta_l + F_{xfr}\sin\delta_r + F_{yfr}\cos\delta_r + F_{yrl} + F_{yrr} = ma_y \qquad (2.6)$$

- Vehicle's rotational equilibrium around the z axle (yaw moment):

$$\begin{aligned} &a(F_{xfl}\sin\delta_l + F_{yfl}\cos\delta_l + F_{xfr}\sin\delta_r + F_{yfr}\cos\delta_r) + \\ &\quad + \frac{t_f}{2}(F_{xfr}\cos\delta_r - F_{yfr}\sin\delta_r - F_{xfl}\cos\delta_l + F_{yfl}\sin\delta_l) + \\ &+ \frac{t_r}{2}(F_{xrr} - F_{xrl}) - b(F_{yrl} + F_{yrr}) + M_{zfl} + M_{zfr} + M_{zrl} + M_{zrr} = I_z\ddot{\psi} \end{aligned} \qquad (2.7)$$

  where M_{zij} are the wheel aligning moments. Integrating this equation, it is possible to obtain the yaw-rate $\dot{\psi}$.

Vehicle velocities can be derived from lateral and longitudinal accelerations and yaw-rate through the relationships described in (2.8):

$$\begin{cases} V_x = \int (a_x + V_y\dot{\psi})dt \\ V_y = \int (a_y - V_x\dot{\psi})dt \end{cases} \qquad (2.8)$$

Knowing the two components, vehicle's overall velocity and *side-slip* angle can be calculated:

$$\begin{aligned} V &= \sqrt{V_x^2 + V_y^2} \\ \beta &= \tan^{-1}\frac{V_y}{V_x} \end{aligned} \qquad (2.9)$$

Vehicle CG accelerations influence the value of vertical forces which act on each corner of the vehicle: they cause load transfer between front and rear axles or left and right vehicle sides, which should be taken into account in the vehicle model.

The presence of a lateral acceleration produced by tire cornering forces generates an inertial reaction force, called *centrifugal force*. It causes a roll motion and, as a consequence, a lateral load transfer. The roll angle ϕ can be evaluated through the moment equilibrium of sprung mass around vehicle roll centre, considering a

horizontal roll axis:

$$I_r\ddot{\phi} + C\dot{\phi} + K\phi = ma_y H_{roll}\cos\phi + mgH_{roll}\sin\phi \quad (2.10)$$

$$ma_y = ma_{y,RC} + H_{roll}\ddot{\phi} \quad (2.11)$$

Where K and C are respectively the vehicle total roll stiffness and total roll damping:

$$\begin{aligned} K &= K_{front} + K_{rear} \\ C &= C_{front} + C_{rear} \end{aligned} \quad (2.12)$$

Substituting (2.11) into (2.10),

$$\ddot{\phi} = \frac{mH_{roll}\left(a_{y,RC}\cos\phi + g\sin\phi\right) - C\dot{\phi} - K\phi}{I_r + mH_{roll}{}^2} \quad (2.13)$$

Integrating two times (2.13), the roll angle is calculated.

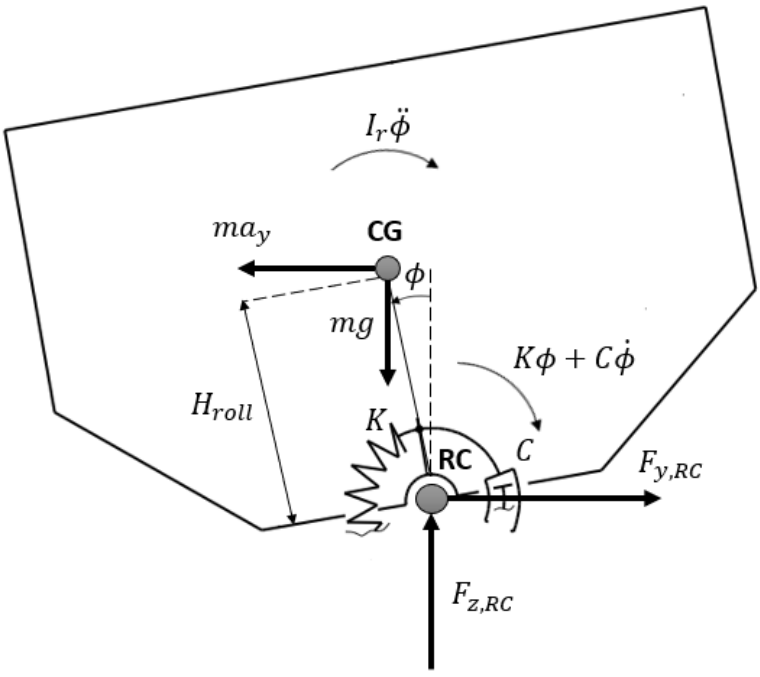

Figure 4: Sprung mass roll equilibrium (adapted from [20])

The lateral load transfer due to this roll motion is obtained through the equilibrium of unsprung mass:

$$F_{zl}T - mg\frac{T}{2} - ma_yH_{RC} = C\dot{\phi} + K\phi \tag{2.14}$$

$$\begin{cases} F_{zl} = \dfrac{mg}{2} - \dfrac{C\dot{\phi} + K\phi}{T} - \dfrac{ma_yH_{RC}}{T} \\ F_{zr} = \dfrac{mg}{2} + \dfrac{C\dot{\phi} + K\phi}{T} + \dfrac{ma_yH_{RC}}{T} \end{cases} \tag{2.15}$$

It follows that the vehicle total lateral load transfer is defined as:

$$\Delta F_{z,lat} = \frac{C\dot{\phi} + K\phi}{T} + \frac{ma_yH_{roll}}{T} \tag{2.16}$$

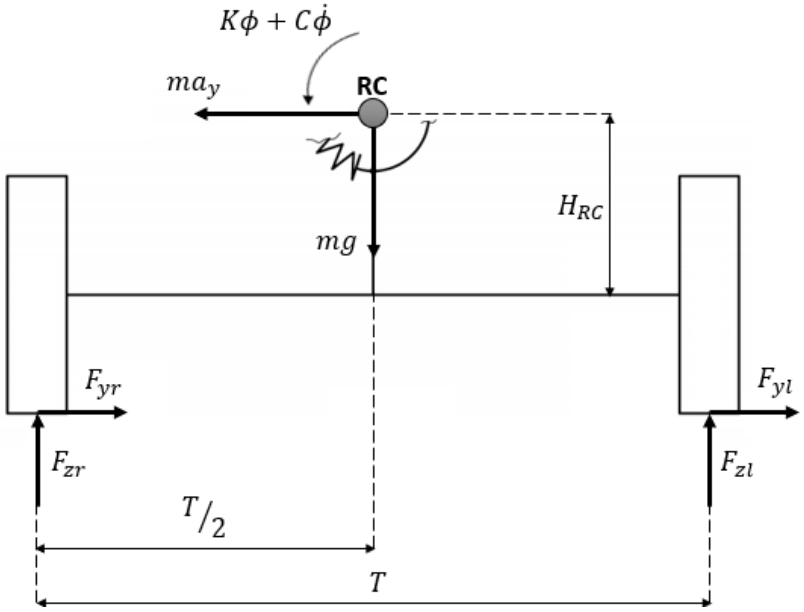

Figure 5: Lateral load transfer (adapted from [20])

It is distributed between the front and rear axles through the corresponding roll stiffnesses, due to suspensions springs and anti-roll bars, and dampings, due to suspensions dampers:

$$\begin{cases} \Delta F_{z,lat,f} = \dfrac{C_f\dot{\phi} + K_f\phi}{T_f} + \dfrac{m_fa_yH_{roll,f}}{T_f} \\ \Delta F_{z,lat,r} = \dfrac{C_r\dot{\phi} + K_r\phi}{T_r} + \dfrac{m_ra_yH_{roll,r}}{T_r} \end{cases} \tag{2.17}$$

In the same way, the presence of a positive longitudinal acceleration due to driving traction condition generates an inertial reaction force, which causes a pitch motion and a longitudinal load transfer:

$$\Delta F_{z,long} = \frac{m a_x h_G}{l} \tag{2.18}$$

Along longitudinal direction, also the aerodynamic resistance causes a longitudinal load transfer:

$$\Delta F_{z,aer} = \frac{\frac{1}{2}\rho C_x A_f V_x^2 \mathrm{sgn} V_x}{l} h_A \tag{2.19}$$

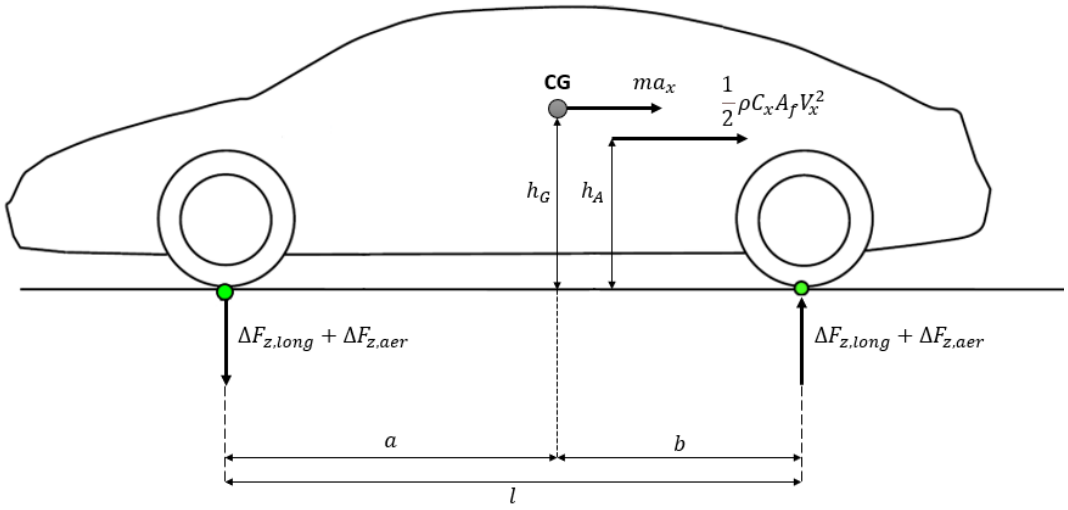

Figure 6: Longitudinal load transfer – driving condition (adapted from [20])

After adding load transfers to the forces due to static load distribution and aerodynamic downforce, the overall vertical forces on each vehicle corner are reported in (2.20):

$$\begin{cases} F_{zfl} = \frac{1}{2}\frac{mgb}{l} + \frac{1}{2}\left(\frac{1}{2}\rho C_{z,f} A_f V_x^2\right) - \frac{1}{2}\left(\Delta F_{z,long} + \Delta F_{z,aer}\right) - \Delta F_{z,lat,f} \\ F_{zfr} = \frac{1}{2}\frac{mgb}{l} + \frac{1}{2}\left(\frac{1}{2}\rho C_{z,f} A_f V_x^2\right) - \frac{1}{2}\left(\Delta F_{z,long} + \Delta F_{z,aer}\right) + \Delta F_{z,lat,f} \\ F_{zrl} = \frac{1}{2}\frac{mga}{l} + \frac{1}{2}\left(\frac{1}{2}\rho C_{z,r} A_f V_x^2\right) + \frac{1}{2}\left(\Delta F_{z,long} + \Delta F_{z,aer}\right) - \Delta F_{z,lat,r} \\ F_{zrr} = \frac{1}{2}\frac{mga}{l} + \frac{1}{2}\left(\frac{1}{2}\rho C_{z,} A_f V_x^2\right) + \frac{1}{2}\left(\Delta F_{z,long} + \Delta F_{z,aer}\right) + \Delta F_{z,lat,r} \end{cases} \tag{2.20}$$

2.3 Handling diagrams

Vehicle handling performance, so how the vehicle behaves with respect to a steering driver demand, has great importance to assess vehicle stability: for this purpose, some characteristics are used to study it.

To understand their significance, a simplified vehicle model can be exploited: the single-track model, also called the *bicycle* model. It permits to evaluate with good approximation how front and rear tire cornering stiffnesses and CG location along wheelbase influence vehicle cornering behaviour. A bicycle model equivalent to the real four-wheel vehicle can be obtained using real axle characteristics, such as axle cornering stiffnesses, which take into account the effects of suspensions and steering compliance, load transfers and body roll [21].

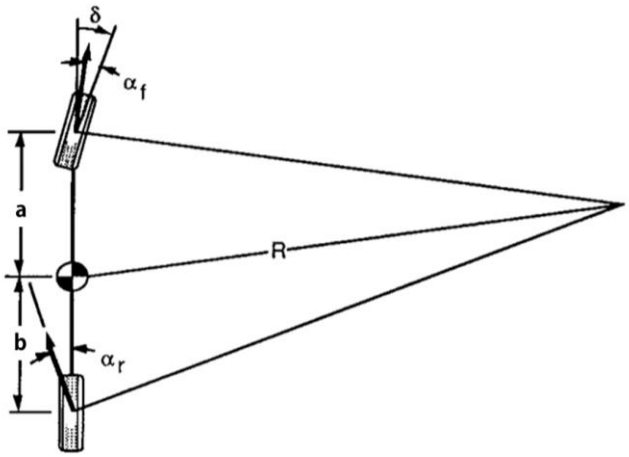

Figure 7: Bicycle vehicle model cornering (adapted from [22])

Bicycle model equations reported in this paragraph are taken from [22] and [23].

In low-speed steering, lateral acceleration can be neglected, so there are no lateral forces at wheels and, consequently, no wheel side slip angles: vehicle wheels are supposed to be in pure rolling condition. This condition is called *kinematic steering*.

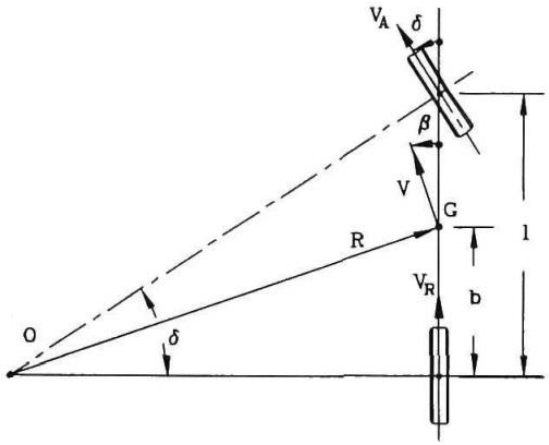

Figure 8: Kinematic steering (adapted from [23])

From Figure 8 vehicle scheme, if vehicle wheelbase can be considered negligible compared to the radius of turn,

$$R \approx l \cot \delta \approx \frac{l}{\delta} \;\Rightarrow\; \delta_{kin} = \frac{l}{R} \tag{2.21}$$

$$R \approx b \cot \beta \approx \frac{b}{\beta} \;\Rightarrow\; \beta_{kin} = \frac{b}{R} \tag{2.22}$$

When vehicle speed cannot be considered small, a lateral acceleration is present; as a consequence, wheels have lateral slip angles different from zero and generate lateral forces: this condition is called *dynamic steering*.

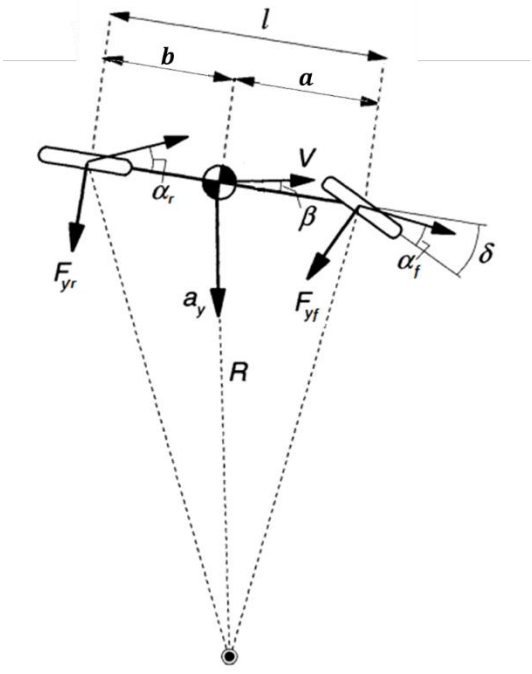

Figure 9: Dynamic steering (adapted from [21])

In a steady-state condition, so when the vehicle is travelling at a constant speed V, and considering small angles ($R \gg l$), the forces in lateral direction must balance the centrifugal force due to lateral acceleration:

$$F_{yf} + F_{yr} = ma_y = m\frac{V^2}{R} \tag{2.23}$$

For the moment equilibrium around the centre of gravity,

$$F_{yf}a - F_{yr}b = 0 \Rightarrow F_{yf} = F_{yr}\frac{b}{a} \tag{2.24}$$

Substituting (2.24) in lateral equilibrium (2.23),

$$\begin{cases} F_{yr} = m\dfrac{V^2}{R}\dfrac{a}{L} = m_r\dfrac{V^2}{R} \\ F_{yf} = m\dfrac{V^2}{R}\dfrac{b}{L} = m_f\dfrac{V^2}{R} \end{cases} \tag{2.25}$$

Considering to be in the linear region of the curve $F_y(\alpha)$, which is valid for small wheel lateral angles, for each axle the lateral force is obtained as the product of wheel lateral slip angle and the corresponding *cornering stiffness*:

$$\begin{cases} F_{yr} = C_{\alpha r}\alpha_r \\ F_{yf} = C_{\alpha f}\alpha_f \end{cases} \tag{2.26}$$

Substituting (2.26) in lateral force expression (2.25),

$$\begin{cases} \alpha_r = \dfrac{m_r}{C_{\alpha r}}\dfrac{V^2}{R} \\ \alpha_f = \dfrac{m_f}{C_{\alpha f}}\dfrac{V^2}{R} \end{cases} \tag{2.27}$$

From simple geometrical relationships of vehicle angles,

$$\delta = \delta_{kin} + \alpha_f - \alpha_r \tag{2.28}$$

Substituting (2.27) in (2.28),

$$\delta - \delta_{kin} = \left(\frac{m_f}{C_{\alpha f}} - \frac{m_r}{C_{\alpha r}}\right)\frac{V^2}{R} = UG\frac{V^2}{R} \tag{2.29}$$

The lateral acceleration coefficient in (2.29), called *Understeer Gradient*, is the most commonly used handling parameter: its value permits to characterize vehicle cornering behaviour. It defines how the steering angle δ has to be changed, in terms of magnitude and direction, with the trajectory radius or lateral acceleration [22]; the corresponding handling diagram is the plot of δ as a function of a_y:

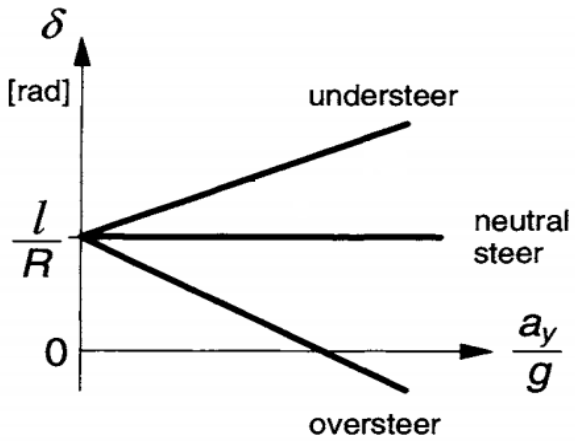

Figure 10: Steer angle versus lateral acceleration at constant path curvature (adapted from [21])

The value of Understeer Gradient permits to distinguish three conditions of vehicle behaviour [22][24][25]:

- Understeer: $UG > 0$, so it is necessary to increase the steering angle linearly with lateral acceleration, or with the square of the speed at a constant radius turn; this means that the front wheel lateral slip angle is higher than the rear wheel one; a vehicle configuration is called *understeer* when, at the same lateral acceleration applied to the CG and same steering angle, the radius of the CG turn trajectory is higher than kinematic condition;

- Neutral steer: $UG = 0$, so the steering angle does not change when lateral acceleration increases (increasing speed at constant radius or reducing radius at constant speed); a vehicle configuration is called *neutral steer* when, as lateral acceleration is applied to vehicle CG, it follows the same geometric kinematic condition path;

- Oversteer: $UG < 0$, so the steering angle has to decrease linearly with lateral acceleration, and the rear wheel lateral slip angle increases more than the

front wheel one; a vehicle configuration is called *oversteer* when, at the same lateral acceleration applied to the CG and same steering angle, the radius of the CG turn trajectory is lower than kinematic condition. Oversteer vehicles are characterized by a *critical speed*, above which they develop unstable behaviour:

$$V_{crit} = \sqrt{-\frac{l}{UG}} \tag{2.30}$$

Handling parameters and diagrams can be evaluated during a *ramp steer* manoeuvre: after setting vehicle speed value, that has to be maintained constant during all the test, the steering is gradually increased, like a ramp. The values of handling performance parameters are calculated at the linear range of tire performance; all gradient values are obtained measuring the slope of corresponding handling diagrams curves.

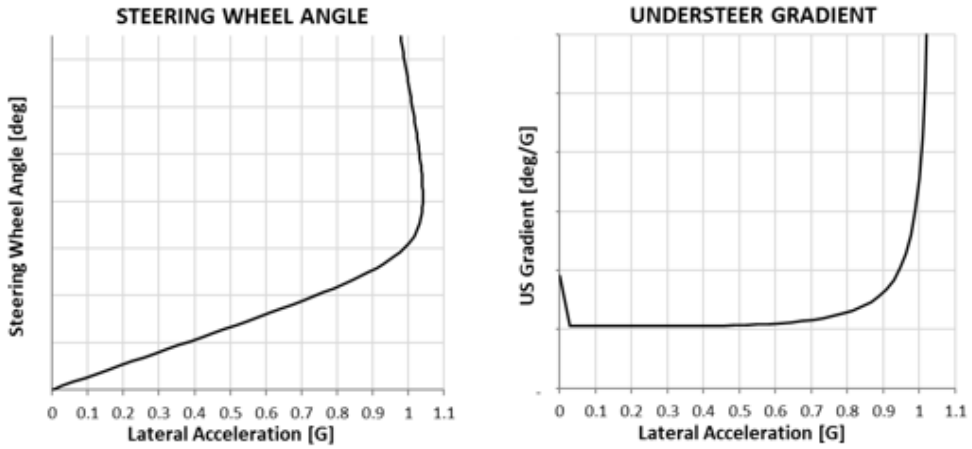

Figure 11: Understeer gradient evaluation during a ramp-steer manoeuvre

Similarly to the steering angle, it is possible to calculate vehicle side-slip angle β during dynamic steering starting from geometrical relationships:

$$\beta = \beta_{kin} - \alpha_r \tag{2.31}$$

$$\beta - \beta_{kin} = -\frac{m_r}{C_{\alpha r}}\frac{V^2}{R} \tag{2.32}$$

The coefficient $(-m_r/C_{\alpha r})$ in (2.32) is called *Side-Slip Gradient*: it defines how vehicle side-slip angle changes with lateral acceleration during cornering, or with

the radius of turn considering a constant speed condition. It can be considered a second index to define vehicle handling behaviour; the corresponding handling diagram indicates a_y on the abscissa axis and β on the vertical axis.

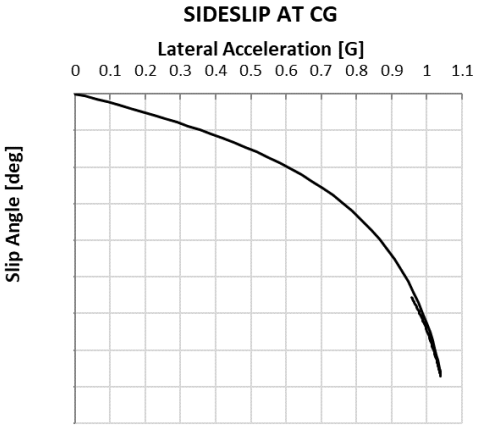

Figure 12: Side-Slip angle diagram for a ramp-steer manoeuvre

A third index that provides information about vehicle understeer or oversteer behaviour of a bicycle model is the *Static Margin*. It is based on the definition of vehicle's *Neutral-steer Point:* the point along the chassis at which an external lateral force can be applied without producing a steady-state yaw velocity ($\dot{\psi} = 0$), under the assumption of no steer ($\delta = 0$) [24]. In these conditions, the lateral forces on the front and rear axle are respectively equal to $C_{\alpha f}\beta$ and $C_{\alpha r}\beta$ [25], and the longitudinal coordinate of the *Neutral Point* is:

$$x_N = \frac{aC_{\alpha f} - bC_{\alpha r}}{C_{\alpha f} + C_{\alpha r}} \tag{2.33}$$

The Static Margin is defined as the difference between x_N and longitudinal position of vehicle CoG, normalized with respect to vehicle wheelbase [25]:

$$SM = \frac{x_N - a}{l} \tag{2.34}$$

It follows that for a Neutral Steer vehicle the Neutral Point coincides with the CoG, so the Static Margin is equal to zero; for an Understeer vehicle the Neutral point is behind the CoG, so the Static Margin is positive; for an Oversteer vehicle the Neutral Point is ahead of the CoG, so the Static Margin is negative [24]. Here too, the related handling diagram shows the relationship between SM and lateral acceleration a_y.

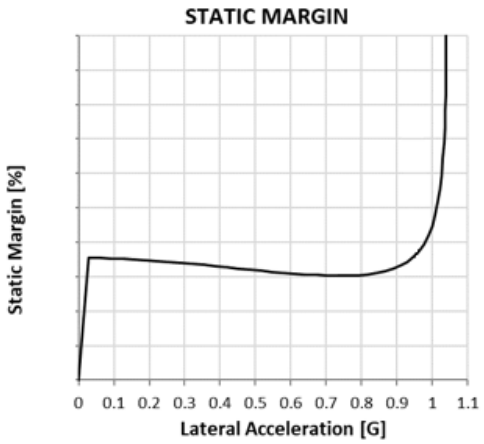

Figure 13: Static Margin diagram for a ramp-steer manoeuvre

The last two handling diagrams considered in this study are the *Roll Gradient* and the *Lateral Load Transfer Distribution % Front* (*LLTD* [%*F*]). From the bicycle model it is not possible to evaluate vehicle body roll and lateral load transfer; hence it is necessary to consider the four-wheel model to measure them. Also for these parameters the related handling diagrams report their values as functions of lateral acceleration.

Vehicle Roll Gradient defines how body roll angle changes with respect to vehicle lateral acceleration, hence it is a function of vehicle total roll stiffness. It can be used as a target during the vehicle design process, defining a desirable value.

As seen in handling equations reported in the previous paragraph, vehicle body roll is related to vehicle total lateral load transfer. Lateral load transfer division between vehicle axles depends on how total roll stiffness is distributed between the front and rear tracks, and has a huge influence on the vehicle under/oversteer behaviour. In conclusion, LLTD [%F] can be considered an additional handling parameter to be taken into account for vehicle design.

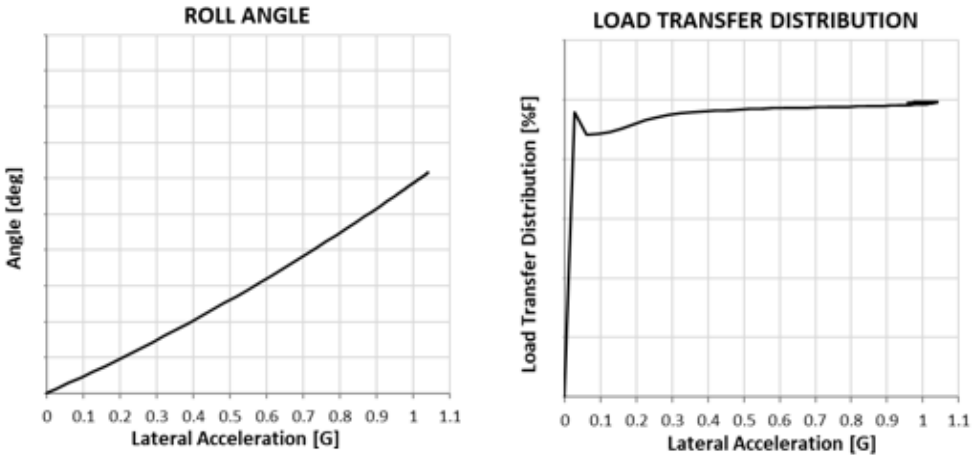

Figure 14: Roll angle and LLTD [%F] diagrams for a ramp-steer manoeuvre

2.4 Tire dynamics

For each wheel, the dynamic equilibrium around its centre is described by (2.35), where the single degree of freedom is its angular speed:

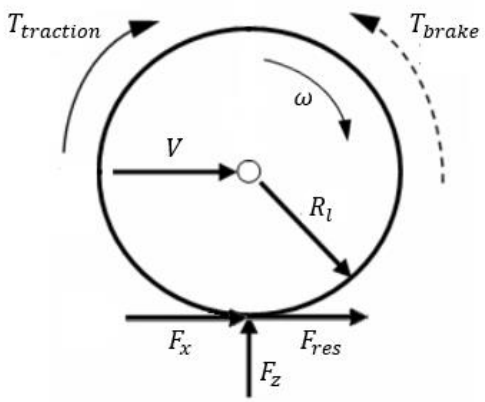

Figure 15: Wheel free body diagram (adapted from [19])

$$I_W\dot{\omega} = T_{traction} - T_{brake} - F_{res}R_l - F_xR_l \tag{2.35}$$

Where:

- I_W is the wheel inertia;
- $T_{traction}$ is the traction torque;
- T_{brake} is the brake torque;
- R_l is the tire *loaded radius*, calculated as the difference between undeformed radius and the vertical deflection due to the vertical load on tire (obtained

through tire's *vertical stiffness* k_v):

$$R_l = R_w - \frac{F_{z,tire}}{k_v} \tag{2.36}$$

- F_{res} is the rolling resistance of the wheel, defined as the product between wheel's vertical load on the tire and a rolling coefficient (a polynomial function of vehicle speed):

$$F_{res} = (f_0 + f_1 V + f_2 V^4) F_{z,tire} \tag{2.37}$$

- F_x is the longitudinal force transmitted by the tire to the ground; its value depends on wheel vertical load, friction coefficient with the ground, tire characteristics and longitudinal deformation during vehicle motion.

Considering a wheel rolling on a level road without applying on it a braking or tractive torque (pure rolling condition), the *rolling radius* R_e, lower than tire undeformed radius R_w, is defined as the ratio between the longitudinal speed of the wheel V and its angular speed ω_0:

$$R_e = \frac{V}{\omega_0} \tag{2.38}$$

If on the rolling wheel a braking torque is applied, due to tire deformability the new rolling radius R'_e is higher than R_e, and the angular velocity ω lower than ω_0; in the same way if a tractive torque is applied on the wheel, R'_e is lower than R_e, and ω higher than ω_0 [23].

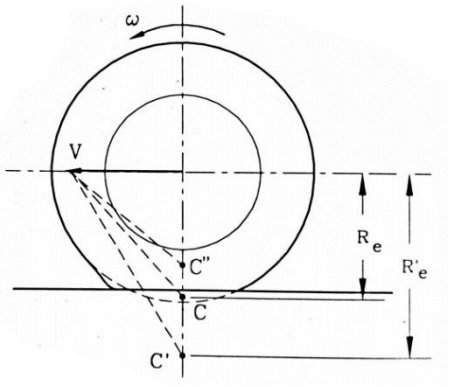

Figure 16: Position of wheel centre of rotation in pure rolling (C), breaking (C') and traction (C'') condition [23]

To evaluate the magnitude of tire's longitudinal deformation, so the difference of tire condition compared to pure rolling, *longitudinal slip* S is defined:

$$S = \frac{R_e\omega - V}{\max(V, R_e\omega)} \tag{2.39}$$

- during braking, $V > R_e\omega$, so $0 > S > -1$
- during traction, $V < R_e\omega$, so $1 > S > 0$

The presence of a not negligible longitudinal slip on the tire contact patch generates a longitudinal wheel ground force.

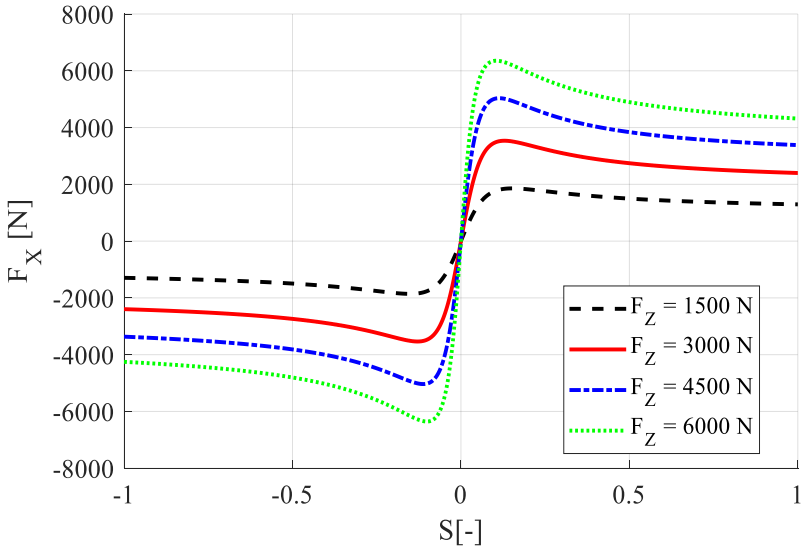

Figure 17: Curves $F_x(S)$ for different load values for a tire 225/50 R 17 [20]

In the same way, the tire exerts a lateral force when there is a lateral deformation, detected by the wheel *side slip angle* (or *lateral slip angle*) α:

$$\tan\alpha = \frac{V_{cy}}{V_{cx}} \tag{2.40}$$

where V_{cy} and V_{cx} are respectively lateral and longitudinal velocities of the wheel centre, so by definition α is the angle between wheel longitudinal midplane and wheel velocity direction.

The resultant lateral force F_y is generally applied at a distance from the centre of the contact patch, called *pneumatic trail* t. As a consequence, it causes a *self-aligning moment* $M_z = F_y t$ which tends to align the wheel longitudinal midplane

with wheel velocity direction, reducing α.

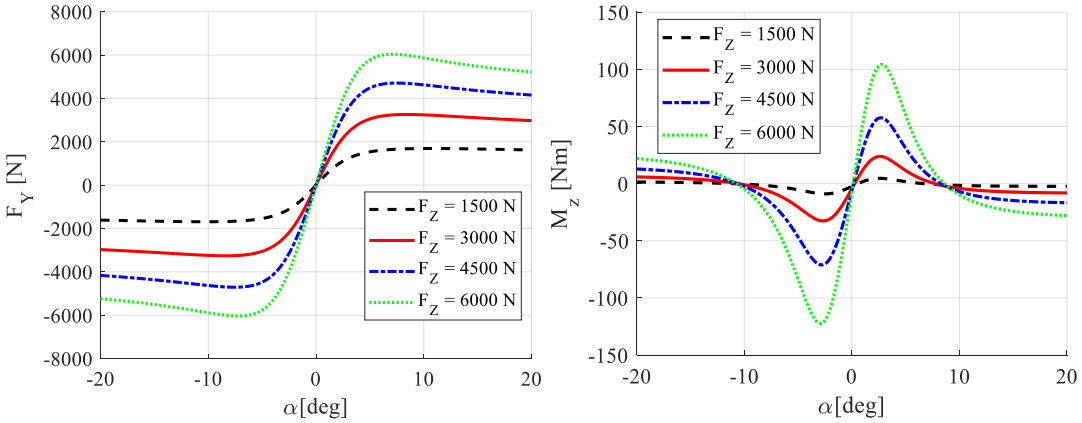

Figure 18: Curves $F_y(\alpha)$ and $M_z(\alpha)$ for different load values for a tire 225/50 R 17 [20]

The side-slip angle of each wheel can be calculated from vehicle CG velocities obtained in Paragraph 2.2, knowing front wheels steering angles and neglecting the contribute of wheels toe angles:

$$\begin{cases} \alpha_{fl} = \tan^{-1}\left(\dfrac{v_y + l_f\dot{\psi}}{v_x - \dfrac{w}{2}\dot{\psi}}\right) - \delta_l \\ \alpha_{fr} = \tan^{-1}\left(\dfrac{v_y + l_f\dot{\psi}}{v_x + \dfrac{w}{2}\dot{\psi}}\right) - \delta_r \\ \alpha_{rl} = \tan^{-1}\left(\dfrac{v_y - l_r\dot{\psi}}{v_x - \dfrac{w}{2}\dot{\psi}}\right) \\ \alpha_{rr} = \tan^{-1}\left(\dfrac{v_y - l_r\dot{\psi}}{v_x + \dfrac{w}{2}\dot{\psi}}\right) \end{cases} \quad (2.41)$$

Generally, the tire is in a combined slip condition, and this influences its behaviour in terms of maximum forces values: applying a tractive or braking force to a tire with a side-slip angle different from zero, a reduction of lateral force value occurs. In the same way, when a lateral force is developed between the tire and the ground, the maximum longitudinal force value is lower than pure longitudinal slip condition [23].

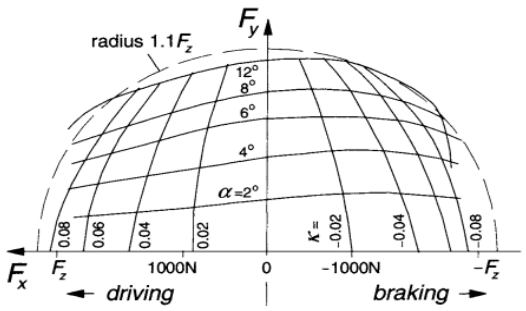

Figure 19: $F_y - F_x$ characteristic for combined slip [21]

Different mathematical theories and functions have been developed to correctly predict tire performances in terms of forces and moments generation, reaching approximations of real forces curves. Among them, the so-called *Magic Formula* tire model, defined by Pacejka, shows a good accuracy in describing tire behaviour: it is a *semi-empirical* model since it is based both on measured data and previous physical models [21].

The model allows obtaining the expressions of wheel ground forces with respect to corresponding slips (longitudinal slip for longitudinal force, side slip for lateral force and self-aligning moment) through an equation like (2.42):

$$y = D\sin\left(C\tan^{-1}\left\{B(x+S_h) - E\left[B(x+S_h) - \tan^{-1}\left(B(x+S_h)\right)\right]\right\}\right) + S_v \qquad (2.42)$$

where y is the output quantity (force), x is the input variable (slip), B is the *stiffness factor*, C is the *shape factor*, D represents the *peak value*, E is the *curvature factor*, S_h is the *horizontal shift* and S_v is the *vertical shift*. The product BCD, called *longitudinal stiffness,* defines the slope of the curve when $x + S_h = 0$ [23]. The values of the coefficients are influenced both by tire characteristics and other model input quantities: camber angle, vertical wheel load, vehicle speed and tire/road friction coefficient. Corrective factors are also introduced to take into account the effects of combined slip.

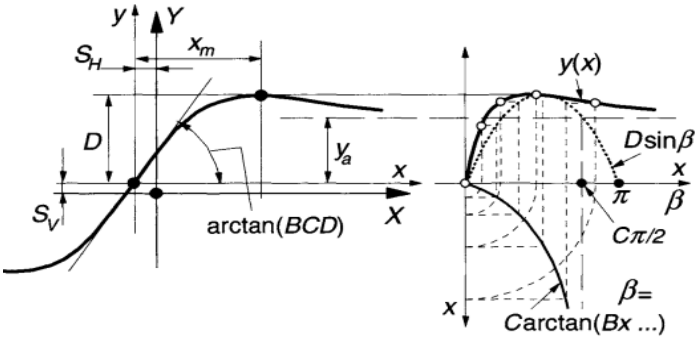

Figure 20: Curve produced by the original sine version of the Magic Formula [21]

3 *VI–CarRealTime*

VI-CarRealTime is a virtual modelling and simulation platform targeted to a simplified four wheels vehicle model. The vehicle model is obtained assembling information from its principal subsystems, such as *body*, *suspensions*, *powertrain*, and its performances are evaluated through dynamic manoeuvre schedules, simulations and results post-processing. The model configuration is defined to accurately predict overall vehicle behaviour for cornering, braking and acceleration performance studies for four-wheeled vehicles with independent-front and independent-rear suspensions [26].

The *VI-CarRealTime* vehicle model is composed of five rigid parts, consisting of vehicle chassis (sprung mass) and four wheels (unsprung masses), and includes 14 DOFs as described in Paragraphs 2.1, 2.2.

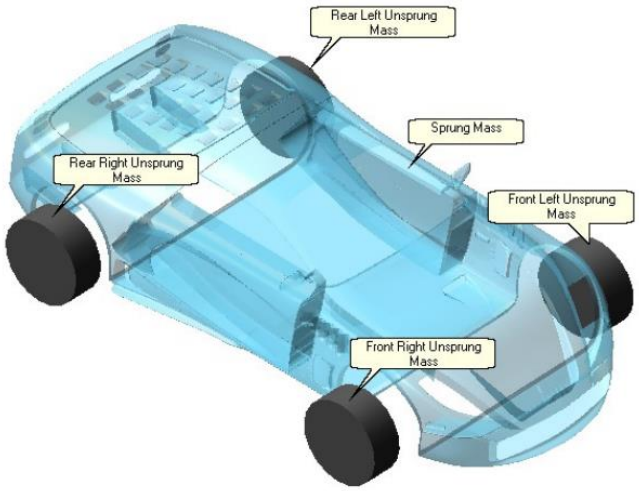

Figure 21: VI-CarRealTime vehicle model [26]

3.1 Vehicle Model on *VI-CarRealTime*

Vehicle system configuration can be defined or changed through setting model data in *VI-CarRealTime Build* mode. In the specific case of the present hybrid vehicle model, the parameters of each subsystem are established in the software environment in order to achieve correlated targets in terms of vehicle behaviour and performance:

- **Body:** in this subsystem information about mass, inertia and setup of vehicle sprung mass can be set. In this case, sprung mass parameters are defined starting from target specifications about the overall vehicle, including the presence of the driver, passenger and fuel, and knowing unsprung masses inertial information:

Vehicle (kerb + 2 passengers + fuel)	
Parameter	**Value**
Mass $[kg]$	1850
Wheelbase $[mm]$	2600
CoG height $[mm]$	490
Weigth distribution %Front [%]	48
Rolling inertia I_{xx} $[kgm^2]$	700
Pitch inertia $I_{yy}[kgm^2]$	2600
Yaw inertia $I_{zz}[kgm^2]$	2900

Table 1: Vehicle parameters

All the vehicle values are defined considering *VI-CarRealTime Vehicle Reference System*:

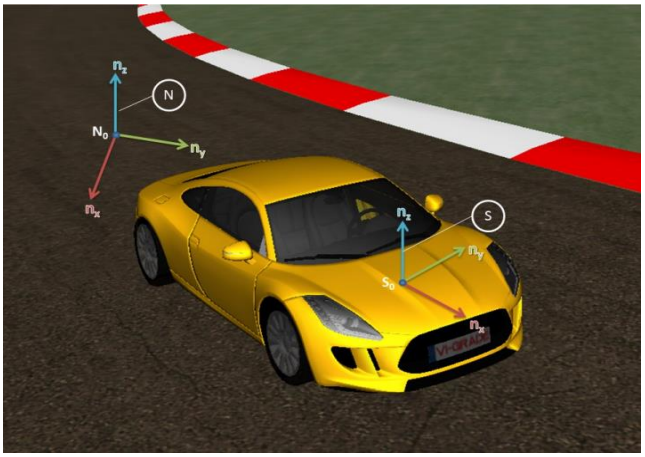

Figure 22: VI-CarRealTime Vehicle Reference System [26]

VI-CarRealTime reference systems are consistent with the standards *ISO 8855* and *SAE Recommended Practice J670f*. As regards *Vehicle* one, the origin S_0 is located at $Z = 0$ of *Global Reference Frame*, as shown in Figure 22, and at half front vehicle track. The axes are oriented, at design time, with $X+$ pointing forward in the direction of motion, $Y+$ pointing leftward, $Z+$ pointing upward [26].

Mass and location of passengers and fuel are known and set in *Body Setup Data Property Editor*:

	Xlocation $[mm]$	**Ylocation $[mm]$**	**Zlocation $[mm]$**	**Mass $[kg]$**
Driver	-1100	350	450	75
Passenger	-1100	-350	450	75
Fuel	-1700	0	400	50

Table 2: Passengers and fuel parameters

As a consequence, sprung mass characteristics which satisfy these conditions are calculated and reported in *Sprung Mass* subsystem *Property Editor*; the sprung mass CoG coordinates are also considered for sensor point location:

Sprung Mass	
Parameter	**Value**
Mass $[kg]$	1418
CG longitudinal front wheel distance $[mm]$	1364
CG height $[mm]$	538
Rolling inertia I_{xx} $[kgm^2]$	509
Pitch inertia $I_{yy}[kgm^2]$	2170
Yaw inertia $I_{zz}[kgm^2]$	2309

Table 3: Sprung mass parameters

- **Powertrain:** this subsystem includes information about vehicle driveline, composed in general by ICE, electric motor(s), clutch, transmission and differentials. The powertrain of the present vehicle is configured as an AWD (All-Wheel-Drive), including a thermal engine which moves the rear axle and two onboard electric motors connected respectively with the two front wheels:

Figure 23: Hybrid vehicle powertrain configuration on VI-CarRealTime

For this specific study, power sources constraints are not considered: the powertrain is designed as if fuel supply for the thermal engine is infinite and as if electric motors are connected to a battery with infinite energy, so all the issues regarding hybrid vehicle energy management (including, for instance, parallel or series configuration, regenerative braking) are not taken into account.

As regards the thermal engine, torque-speed map and gear ratios are defined; it is equipped with an LSD rear differential, whose transmission ratio is 4.8.

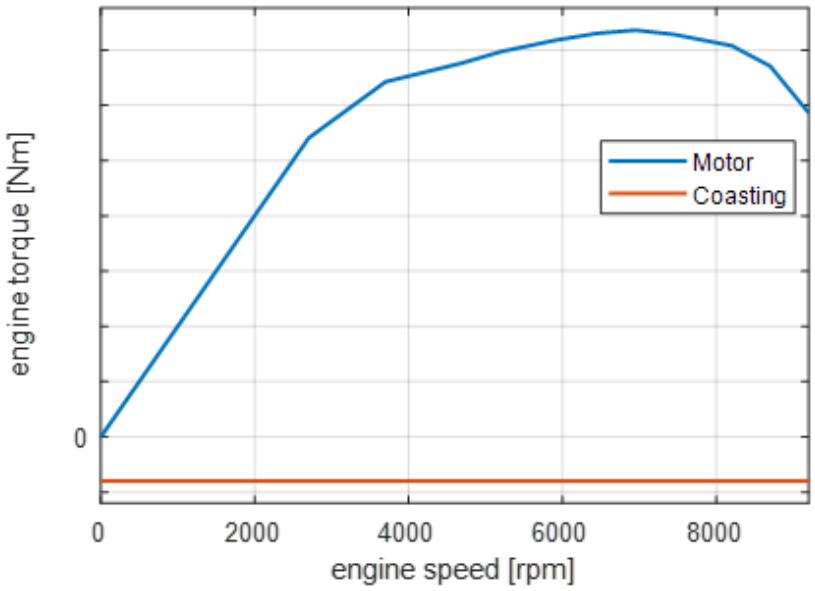

Figure 24: Rear engine torque-speed map

Gear	Gear Ratio
-1	-2.45
0	0.00
1	2.30
2	1.70
3	1.30
4	1.01
5	0.84
6	0.71

Table 4: Transmission Gear Ratios

Regarding LSD differential, in (3.1) the equations that describe how the torque is distributed between the two axle wheels are reported [26]:

$$\begin{aligned} &\delta\omega > 0 \rightarrow T_{left} = \tfrac{1}{2}(T - \delta T), T_{right} = \tfrac{1}{2}(T + \delta T) \\ &\delta\omega < 0 \rightarrow T_{left} = \tfrac{1}{2}(T + \delta T), T_{right} = \tfrac{1}{2}(T - \delta T) \\ &\delta\omega = 0 \rightarrow T_{left} = \tfrac{1}{2}T, T_{right} = \tfrac{1}{2}T \end{aligned} \tag{3.1}$$

When one of the two wheels is spinning more than the other, the differential transfers a higher torque to the low-speed wheel, guaranteeing vehicle traction. Torque correction δT is calculated as shown in (3.2):

$$\begin{aligned} &|\delta T| < |c_0| \rightarrow \delta T = T_{lock} \\ &|\delta T| \geq |c_0| \rightarrow \delta T = \\ &\quad = \begin{cases} c_0 + \delta\omega_{STEP}(c_2|\delta\omega|^{c_3}) & , \quad c_1 T - |c_0| \leq 0 \\ c_0 + \delta\omega_{STEP}(|c_1 T| - |c_0| + c_2|\delta\omega|^{c_3}), & c_1 T - |c_0| > 0 \end{cases} \end{aligned} \tag{3.2}$$

Where:

- $\delta\omega$ is the angular speed difference between left and right wheels;
- $\delta\omega_{STEP} = \text{Step}(\delta\omega, -\omega_{threshold}, \omega_{threshold}, -1,1)$ is a step function including a $\omega_{threshold}$ value used to invert the sign of output torque with continuity when near zero crossing;
- T is the crown wheel torque;
- T_{lock} is the torque value necessary to obtain $\delta\omega = 0$.

When left and right torque difference is lower than c_0, the differential acts like a locked type one (c_0 represents a preload); in the opposite case, δT is obtained through the expression that includes c_0, c_1, c_2, c_3 coefficients. For the specific case, coefficient values are: $c_0 = 10\ Nm$, $0 < c_1 < 0.5$ depending on T value, $c_2 = 0$, $c_3 = 0$, $\omega_{threshold} = 3\ rad/s$, hence the differential behaviour is the same of a locked type one.

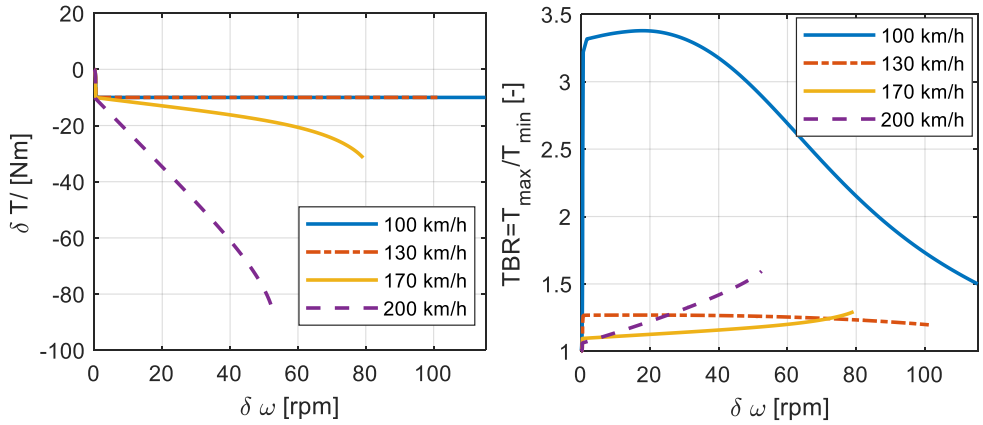

Figure 25: Differential characteristic during rampsteer manoeuvres (20 deg/s @100 km/h, 130 km/h, 170 km/h, 200 km/h)

Electric motors power and transmission ratio are chosen: front left and right wheels are equipped with the same motors, and their transmission ratio to wheel is equal to 3:

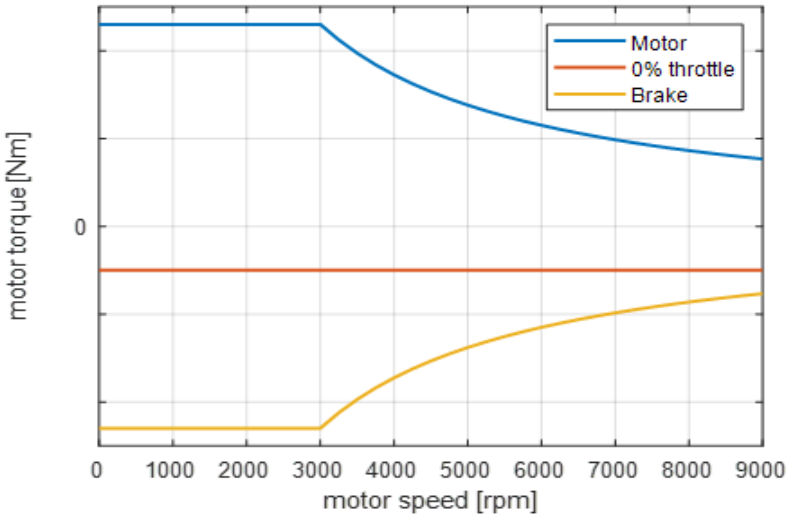

Figure 26: Front electric motor torque-speed map

As regards the division between the front and rear axle torque, there is no fixed ratio: the torque transmitted to the wheels depends to the driver

throttle demand. The throttle pedal command can assume a value included between 0 and 100, representing the percentage of the maximum torque that can be generated by engine and motors at their actual rotational speed. The actual torque value is obtained interpolating between the engine and motor curves corresponding to 0% and 100%.

All the powertrain settings are defined to achieve performance targets in terms of maximum longitudinal acceleration and velocity for a throttle demand step from 0% to 100%:

Target	Value
Maximum longitudinal acceleration $[g]$	0.85
Maximum longitudinal velocity $[km/h]$	330
$0-100\ km/h$ time $[s]$	3.5
$100-200\ km/h$ time $[s]$	6.2
$0-$ max speed time $[s]$	53.0
$0-100\ km/h$ distance $[m]$	47
$100-200\ km/h$ distance $[m]$	272
$0-$ max speed distance $[m]$	3883

Table 5: Acceleration performance targets

- **Brake:** this subsystem is a model of a four-wheel disk brake, in which the parameters can be specified for each wheel independently. The brake system chosen for the present vehicle includes six-piston callipers for front wheels (Figure 27) and four-piston callipers for rear wheels (Figure 28), with the design characteristics, reported in Table 6, taken from a brake system for GT applications:

Element	Front value (left and right)	Rear value (left and right)
Brake pedal ratio [%]	50	50
Master cylinder diameter [mm]	30	30
Calliper acting radius diameter [mm]	152.5	140
Calliper piston 1 diameter [mm]	38	36
Calliper piston 2 diameter [mm]	30	28
Calliper piston 3 diameter [mm]	28	36
Calliper piston 4 diameter [mm]	38	28
Calliper piston 5 diameter [mm]	30	-
Calliper piston 6 diameter [mm]	28	-
Pad friction coefficient [$-$]	0.43	0.47

Table 6: Brake system characteristics

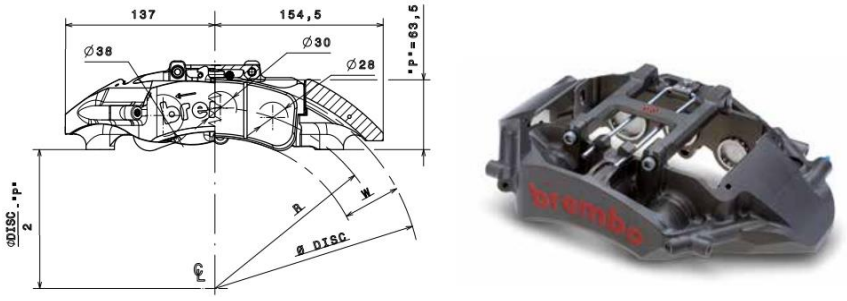

Figure 27: Front brake calliper [27]

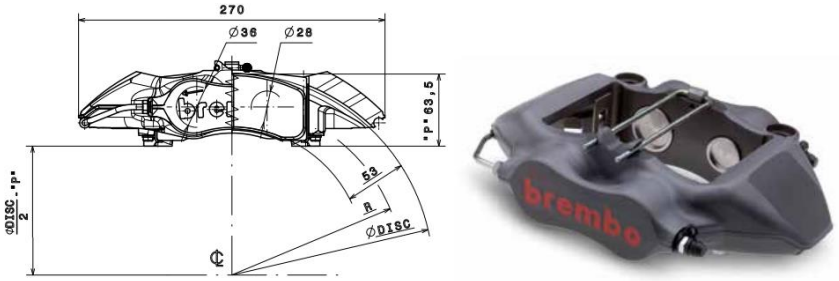

Figure 28: Rear brake calliper [27]

This brake configuration permits to obtain a brake torque distribution front of 60 % and to reach a target maximum longitudinal acceleration of 1.2 g in a $100 - 0$ km/h breaking manoeuvre.

- **Front and rear suspensions:** in *VI-CarRealTime*, suspensions subsystems are described using a conceptual approach: there are no physical part or linkage in the model, but lookup tables describe the suspensions'

behaviour, so computational times are reduced.

The movement of the wheel is related to vertical jounce (independent variable in equations of motion) through a proper constraint in order to define wheel position and orientation (remaining wheel 5 DOFs) by lookup tables. Suspensions kinematic can be modelled as independent, as a function of corresponding single wheel jounce, or dependent, as a function of both left and right wheels jounces. The compliance effect is taken into account considering wheel position and orientation as functions of wheel jounce and external load. The effect of suspension components (springs, dampers, bumpers) is projected onto wheels: lookup tables are used to get element forces applied at the respective component, and a motion ratio from wheel to suspension component travel is exploited to obtain equivalent force at wheel centre [26].

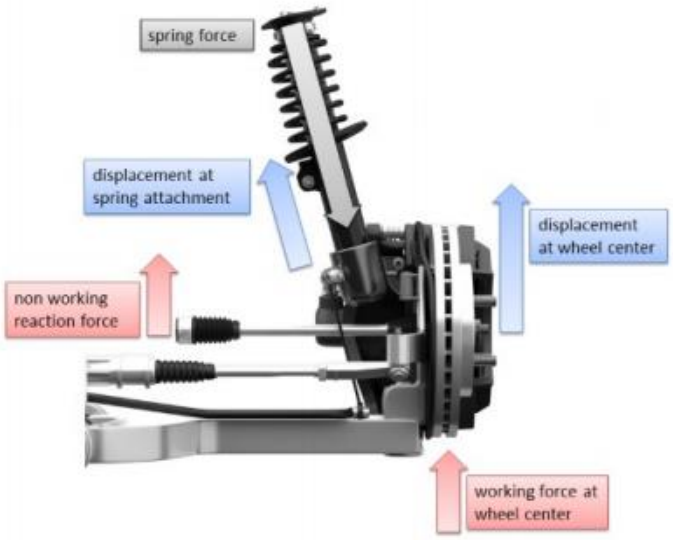

Figure 29: VI-CarRealTime suspension forces evaluation [26]

As regards the vehicle object of this study, the suspensions specifications are modelled importing some K&C results for subsystem lookup tables and defining the components parameters shown in Table 7 and Figure 31:

Wheel location		
	Front	**Rear**
Track $[mm]$	1680	1650
Springs		
	Front	**Rear**
Preload $[N]$	6170	5550
Stiffness $[N/mm]$	85	80
Anti-Roll Bar		
	Front	**Rear**
Stiffness (SWT)$[N/mm]$	26.3	17.5
Bumpers		
	Front	**Rear**
Bumpstop clearance $[mm]$	15.5	26.9
Reboundstop clearance $[mm]$	55	63
Static wheel angles		
	Front	**Rear**
Toe $[deg]$	-0.1	0.15
Camber $[deg]$	-1	-1.5

Table 7: Front and rear suspension characteristics

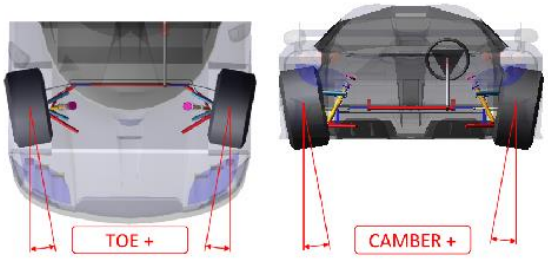

Figure 30: Toe and Camber angles VI-CarRealTime sign reference

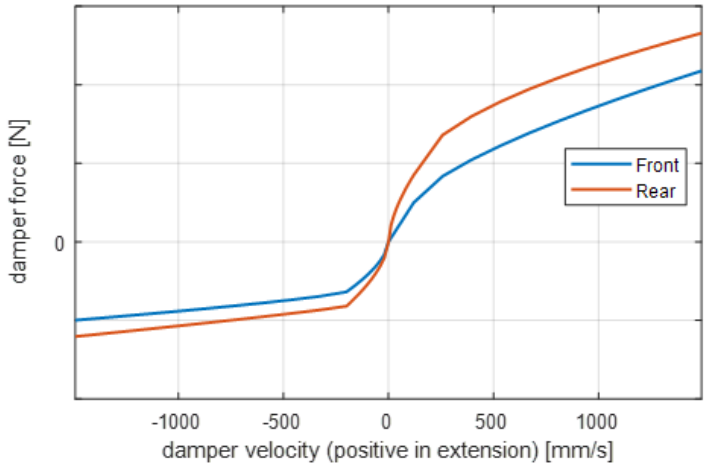

Figure 31: Dampers' characteristics

Springs' preloads are tuned in order to obtain a suspension jounce equal to 0 mm with a tolerance of $\pm 3\ mm$ in static conditions (constant low vehicle's speed), while their stiffnesses influence the slope of curves Force/Jounce at static load. The total Anti-Roll Bar stiffness is defined in order to achieve a target value of roll gradient in a ramp steer manoeuvre of 2.6 deg/g, while its division between front and rear axles leads to a 48 % front lateral load transfer distribution during the same manoeuvre.

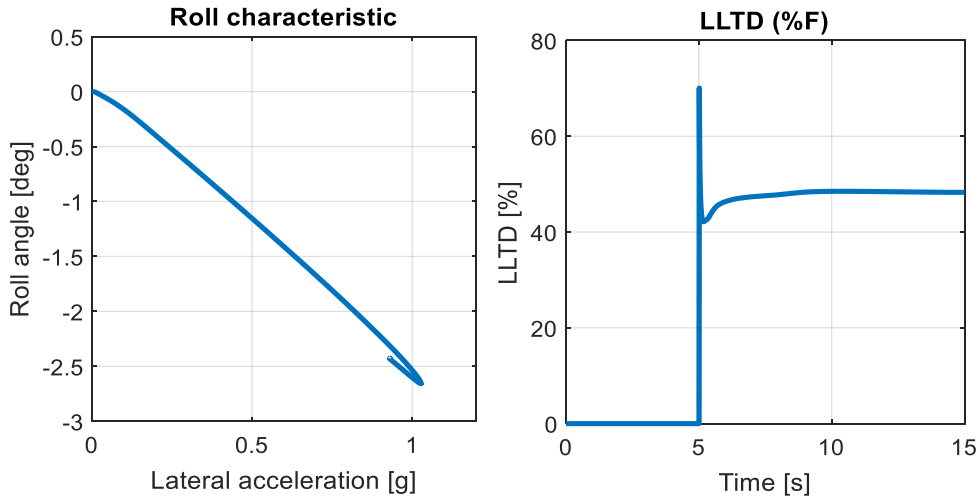

Figure 32: Vehicle's roll characteristics on a rampsteer manoeuvre (20 deg/s @100 km/h)

Bumpstop and reboundstop clearances are obtained considering for both front and rear axles maximum bump travel of 80 mm at a $5g$ vertical load and rebound travel (null vertical load) of 90 mm. This target is verified with a simulation of a parallel wheel travel suspension test, and the result is illustrated in Figure 33:

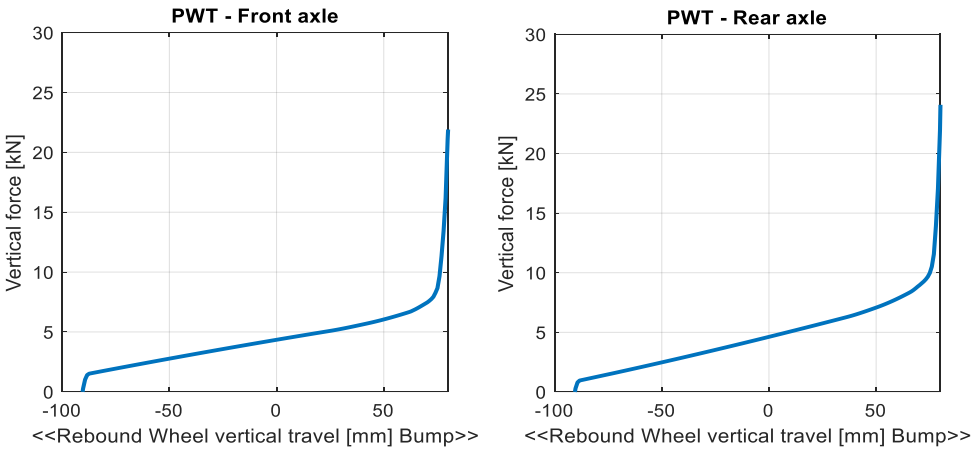

Figure 33: Parallel wheel travel suspension test

- **Front and rear unsprung masses and tires:** these subsystems collect information about mass and inertia of unsprung mass pairs of the vehicle model; they also acquire information about tires' behaviour through *tire property files*, which include tires characteristics defined through coefficients of Pacejka tire model.

  In *tire property files* used for this vehicle, some coefficients, in particular the scaling coefficients λ of Pacejka formulas, are tuned in order to achieve target handling performances (evaluated in a ramp steer manoeuvre): acting on cornering stiffnesses of front and rear tires, an understeer gradient of 56 deg/g and a sideslip gradient of 0.81 deg/g are reached.

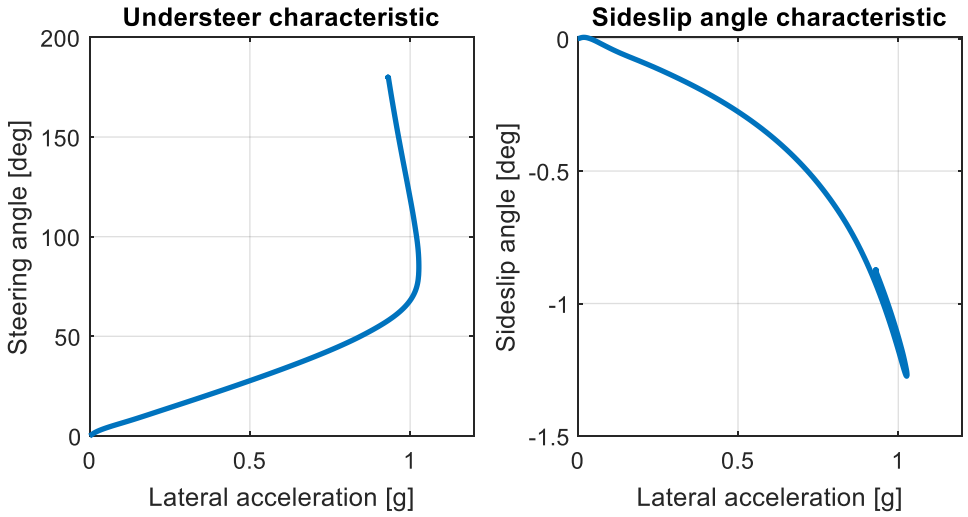

Figure 34: Vehicle's handling characteristics on a rampsteer manoeuvre (20 deg/s @100 km/h)

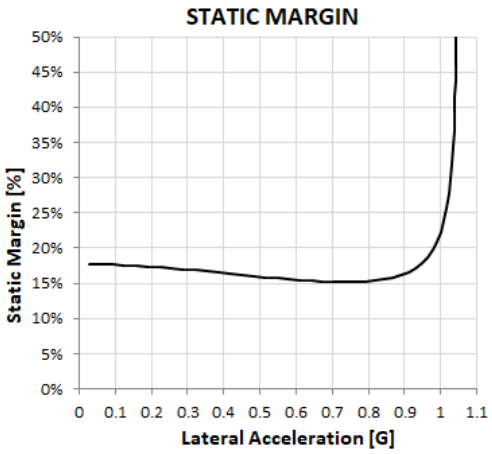

Figure 35: Vehicle's static margin

3.2 Co-simulation with *MATLAB/Simulink*

Through a specific interface, *VI-CarRealTime* environment can interact with *MATLAB/Simulink*: it is possible to connect the vehicle model with *MATLAB* and use *MATLAB* tools to make it more complicated, adding for example control systems or accessories developed in *MATLAB/Simulink* itself. This interface allows the user to run co-simulations and analyse test results.

The *VI-CarRealTime* model is shared with the *MATLAB* environment as an s-function representing the car plant; the s-function receives the car data from *VI-CarRealTime* as a parameter consisting of a file which collects all the model information. Some input and output ports can be specified at the s-function, choosing them from lists of possible channels, so the resulting overall interface is a unique Simulink block that can be connected to other blocks through its ports.

Figure 36: VI-CarRealTime model Simulink block (s-function)

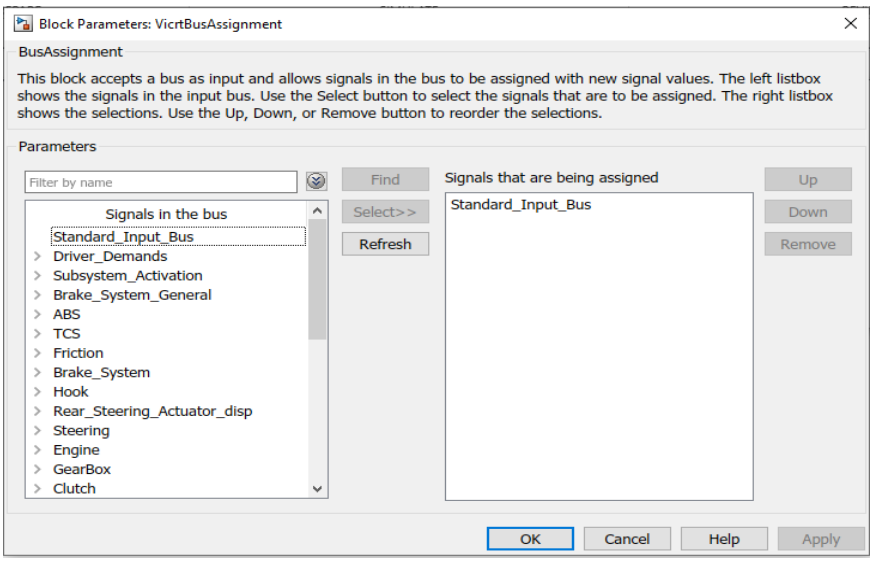

Figure 37: Simulink interface for VI-CarRealTime s-function input ports

To start a co-simulation, the user has first to follow the standard approach on the *VI-CarRealTime* platform as if he has to run a standalone simulation, setting the vehicle model and the manoeuvre event. After making the set-up actions useful to make *MATLAB* s-function communicate with the defined *VI-CarRealTime* event, it is possible to run the co-simulation from the *Simulink* environment.

4 Traction Control System

4.1 Traction Control action

As already mentioned, Traction Control System (TCS) objective is to limit driving wheels longitudinal slip under a threshold value in order to prevent wheels spinning during accelerations, especially with low friction surface road; the control also aims to maintain wheel slip near the optimal value, which corresponds to maximum possible longitudinal wheel ground force [28].

When accelerating, the longitudinal force increases linearly with longitudinal slip, until it reaches a maximum value; if the slip ratio increases further from this point, the force decreases and levels out to a constant value [3][5]. As shown in Figure 38, the part of traction force $F_x(S)$ curve beyond the peak value is considered a zone of instability: during acceleration, if an increasing σ leads to a reduction of F_x value while the traction torque does not reduce, an increasing wheel acceleration is generated (from wheel dynamic equation described in Chapter 2.2); this condition involves wheel spinning [23].

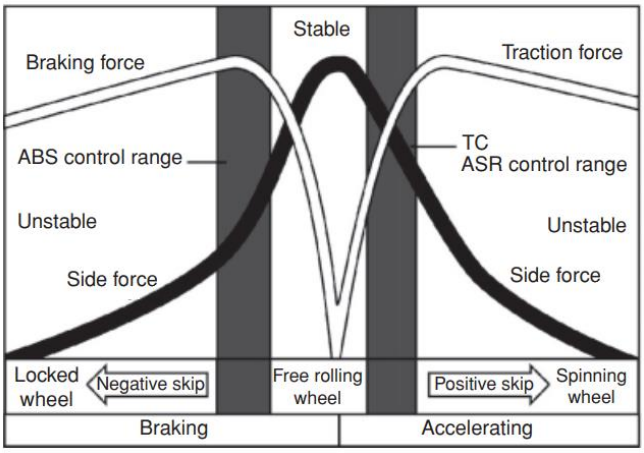

Figure 38: Longitudinal and lateral wheel ground forces as function of longitudinal slip (adapted from [28])

The longitudinal slip value influences also the maximum potential lateral force that the tire can exert: due to the effect of combined slip, there is still sufficient lateral force until longitudinal force reaches its maximum value, while its value goes rapidly to zero for $S \to 1$. As a consequence, out of the threshold value the

vehicle stability is compromised because its force capacity in the lateral direction is severely reduced: spinning front or rear wheels lead respectively to the loss of steering control or directional stability [28]. In this case, an incorrect reaction of the driver causes the loss of vehicle control, in particular on slippery roads or at turns [8].

TCS purpose of keeping the wheel inside the stable slip range is basically obtained with limiting the driving power to the wheel. A proper control has to be precise, dynamic, capable to detect and react to changes of condition in real-time, and robust with respect to external disturbances [30].

The limiting action of TCS maximizes vehicle's longitudinal acceleration both in straight lines and cornering since it enhances the longitudinal performance of driving tires without exceeding their limits [30]. At the same time, it ensures handling stability, guaranteeing satisfactory tire performance in the lateral direction, and so vehicle safety.

4.2 Traction Control Design

The vehicle object of this study presents three different driving modes that can be directly selected by the driver with a switch, depending on environmental conditions and personal driving preferences:

- *Comfort*: it represents the default mode, used for routine drives; the vehicle offers a "middle" performance, balanced between powertrain efficiency and comfort drive feel;
- *Wet*: used in case of rain or adverse conditions in general, when the driver realizes the vehicle shows less traction compared to dry roads; it supports the driver when driving on a slippery road surface, helping him to maintain vehicle stability;
- *Sport*: used on track to reach the maximum of vehicle's dynamic performances, makes the most of the powertrain possibilities.

It follows that the TCS algorithm settings have to be adjusted in order to adapt its operations to the whole vehicle mode performance. In *Comfort* mode, the control operation has to ensure vehicle stability considering generally dry condition

roads. In *Wet* mode the control has to guarantee safety, being more reactive when wheels lose the grip on low-friction roads and limiting the tractive power quickly and much more than *Comfort* mode. In *Sport* mode, the control has to let the vehicle enhance its longitudinal and lateral handling, so its action has to be smoother than *Comfort* mode.

These differences considered, three modes of TCS algorithm are developed; the general scheme of the control for each vehicle wheel is shown in Figure 39:

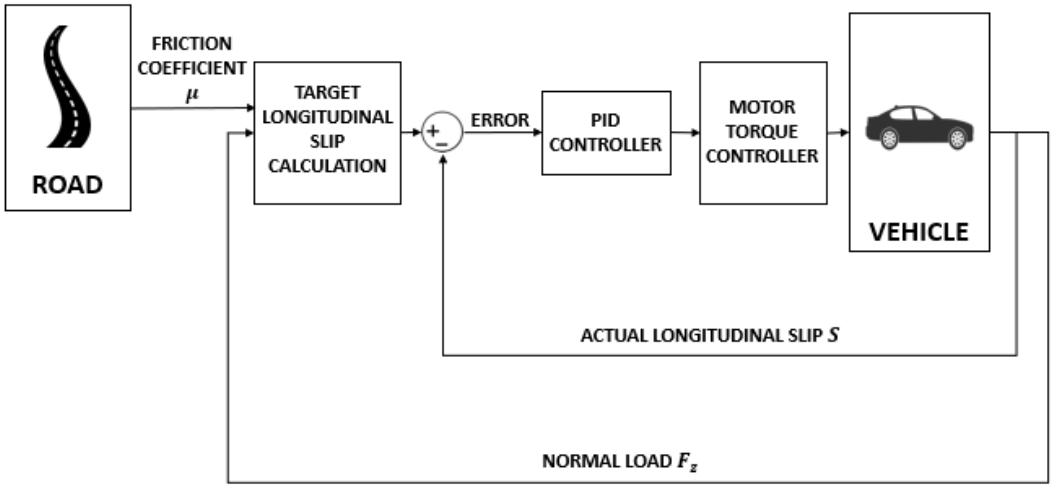

Figure 39: General control scheme for each vehicle wheel

The designed control acts basically on wheel traction torque, limiting powertrain output when the instantaneous wheel longitudinal slip exceeds a threshold value. The actual value of longitudinal slip is compared with the target, calculated as a function of road friction coefficient and wheel vertical load: if the difference is positive, it means that the instantaneous slip is under the threshold, so the control has to remain deactivated and no action is needed on electric motors or engine; on the contrary, if the difference is negative, then the control is activated: the error is elaborated by a PID controller, whose output is a parameter which affects powertrain behaviour (included in "motor torque controller" block in Figure 39 scheme) reducing the traction torque to wheel:

- for front wheels, the output of PID is a subtractive torque which is summed up to the one deriving from driver acceleration demand; the resultant torque, obtained with current control, is the effective one generated by wheel electric motor;
- for rear wheels, the PID acts on throttle valve opening, closing the valve more

than it would be expected from driver acceleration command; in this way, the engine output torque would be lower.

It follows that front wheels can be controlled independently, because each of them is connected to the corresponding electric motor; as a consequence, on front wheels it is possible to optimize longitudinal slip control.

As regards rear wheels, both of them are moved by the engine, thus it is necessary to define which wheel has to be taken as reference for the activation of the control. It also follows that control action itself would not always optimize the slip condition of both the two wheels. In particular, when rear wheels are travelling simultaneously on different friction surfaces: if the control activates referring to the wheel which is spinning more, it will slow down also the wheel that has not yet exceeded the slip limit, penalizing rear axle traction; if the control considers less spinning wheel as the target of activation, it will allow the other wheel to reach high longitudinal slip value, reducing vehicle stability with respect to the previous situation. Based on specific targets of each driving mode, it would be more proper to choose the first or second case.

To avoid the possibility that the control turns repeatedly ON and OFF when the actual longitudinal slip value is around the target one, a hysteresis algorithm is implemented: ON and OFF thresholds have different values and limit a neutral zone that includes the target slip; the control activates when the monitored slip is higher than the upper value and deactivates when it is under the lower one.

4.2.1 Target longitudinal slip calculation

The target longitudinal slip is the value that has to be compared with the instantaneous slip one to determine traction control activation.

As explained in Paragraph 4.1, the wheel longitudinal slip has to remain under the value for which maximum longitudinal force is generated. Considering to be in pure longitudinal slip condition, wheel's ground longitudinal force depends, as well as on longitudinal slip, on wheel's vertical load F_z and road friction coefficient μ. For this study the Pacejka tire model is considered, for which

longitudinal force is expressed by equation (4.1):

$$F_{x0} = D\sin\left(C\tan^{-1}\{B(S+S_h) - E[B(S+S_h) - \tan^{-1}(B(S+S_h))]\}\right) + S_v \qquad (4.1)$$

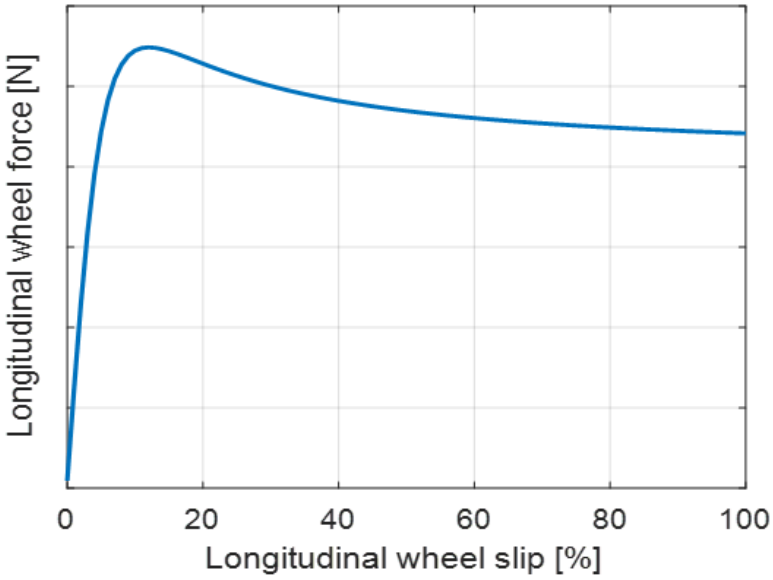

Figure 40: Pacejka $F_{x0}(S)$ curve of vehicle front wheels

Pacejka coefficients of front and rear wheels are considered known. The meaning of each coefficient is explained in Paragraph 2.4; a more detailed description can be found in [21].

Varying normal load and road friction coefficient values, both maximum longitudinal force value and the corresponding slip (target slip) change; the effect of F_z is shown in Figure 41, while the influence of μ is shown in Figure 42:

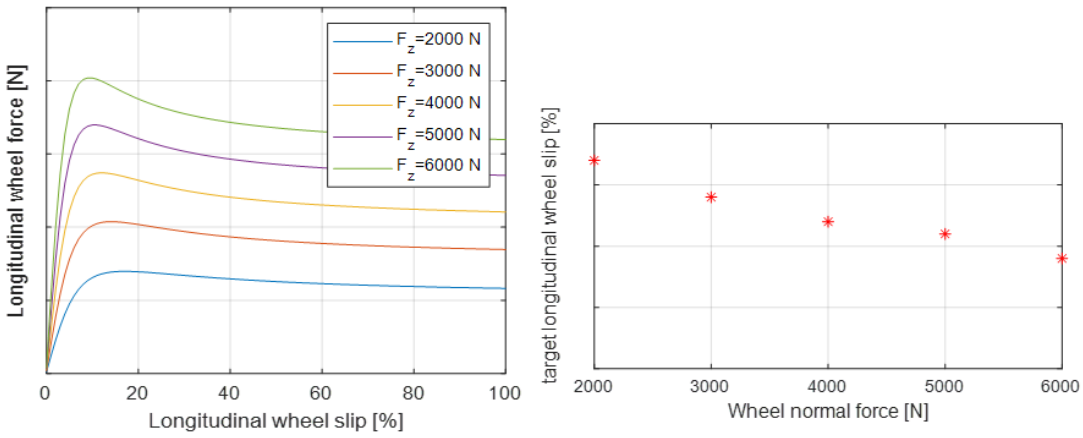

Figure 41: Influence of wheel vertical load on wheel longitudinal force, for $\mu = 1$ (front wheels)

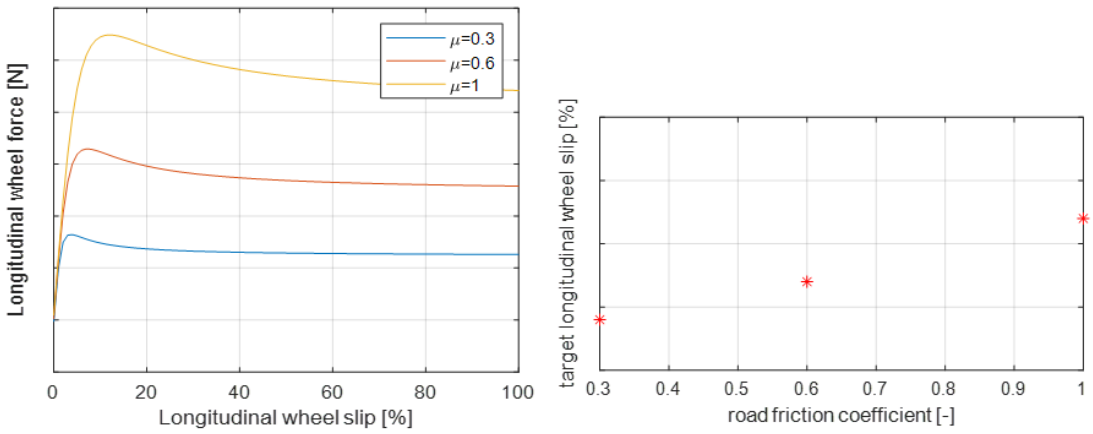

Figure 42: Influence of road friction coefficient on wheel longitudinal force, for $F_z = 4000\ N$ (front wheels)

Analysing graphics results, it can be noticed that increasing the wheel's vertical load, at constant road friction coefficient, the maximum value of wheel longitudinal force increases, and it is obtained for decreasing longitudinal slip value. Increasing the road friction coefficient, keeping constant the wheel's vertical load, maximum longitudinal force, and target longitudinal slip reach higher values.

In order to take into account the influence of both these two parameters, the block "target longitudinal slip calculation" in the control scheme shown in Figure 39 takes as inputs the instantaneous values of F_z and μ, and calculates longitudinal slip value at which maximum wheel longitudinal ground force is reached.

4.2.2 *Comfort* mode

Comfort driving mode is expected to be selected during normal driving conditions: a proper compromise between vehicle traction and safety is required.

Single front wheel control scheme is illustrated in Figure 43:

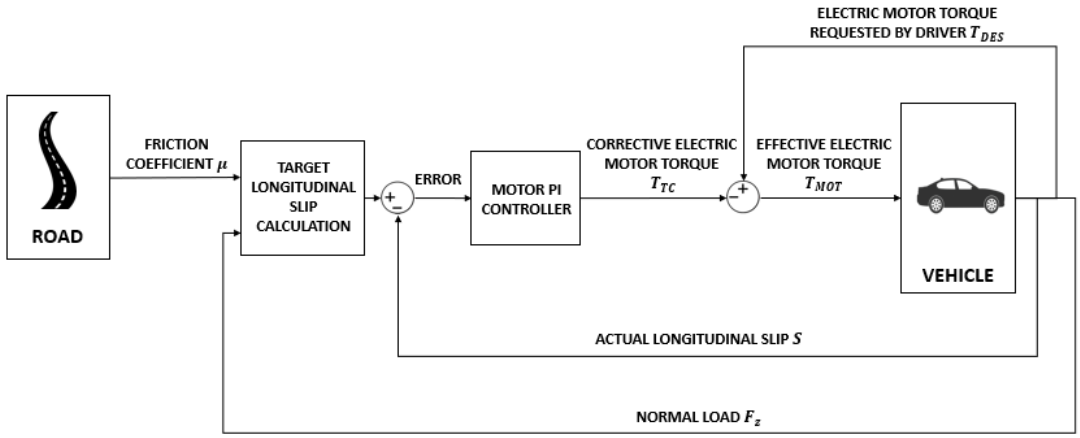

Figure 43: Comfort mode front wheels control scheme

The controller output is defined as "corrective electric motor torque", which is subtracted to the torque required by the driver to prevent wheel spinning during excessive accelerations. The resulting "effective electric motor torque" is requested to wheel motor through current command.

Target longitudinal slip is calculated considering the actual instantaneous road friction coefficient: in this way, the control assures that each front wheel slip value is maintained under a threshold corresponding to the effective maximum longitudinal force.

As regards rear wheels control scheme, it is shown in Figure 44:

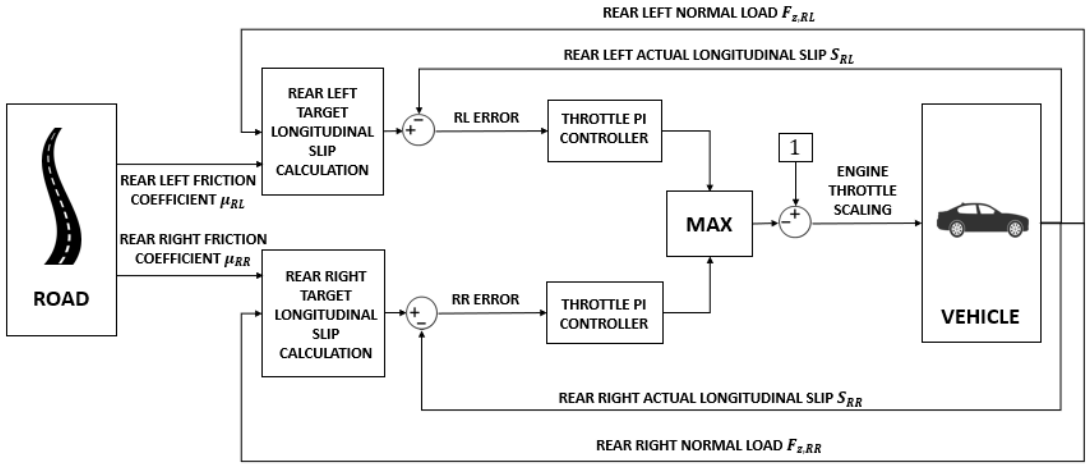

Figure 44: Comfort mode rear wheels control scheme

For the rear axle, the output of PID controller is a value between 0 and 1 which is subtracted to 1 to obtain an "engine throttle scaling" parameter; it represents engine throttle valve opening: when the scaling value is equal to 1, the valve

reaches an opening position which allows the engine to produce a power torque coherent with driver acceleration request; when the scaling value is lower than 1, the valve is less opened with respect to the previous case, so the engine generates a lower output torque.

As previously anticipated, a key point of the rear engine control is the choice of the reference wheel slip, due to the fact that both the speeds of rear wheels are influenced by the torque reduction. For *Comfort* mode, it is essential to guarantee good vehicle stability, as a consequence both the left and right wheels have not to exceed their respective threshold slip values. For this reason, the higher signal between left and right controllers' outputs is sent to throttle scaling command: it is sufficient that one of the two wheels is spinning over its limit to activate the control.

4.2.3 *Sport* mode

When the driver switches to *Sport* driving mode, maximum vehicle performances are required. As regards Traction Control, its action influences vehicle longitudinal dynamics directly; hence, for this mode the control purpose is to reach the maximum vehicle longitudinal acceleration, enhancing traction.

Single front wheel control scheme is reported in Figure 45:

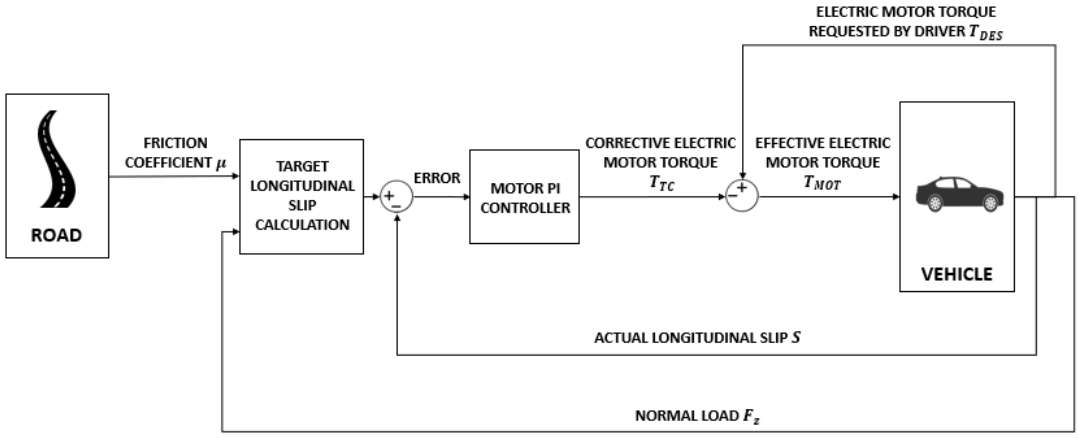

Figure 45: Sport mode front wheels control scheme

It is substantially the same control algorithm of *Comfort* mode: front wheels control is already optimized because each wheel is controlled independently and

reaches the best slip condition. PID coefficients values represent the main difference with respect to *Comfort* mode: in this case, parameters tuning is made in order to obtain a less reactive control; to reach a sport driving feeling, it is preferred to have a smoother control action to let the driver exploiting at maximum the powertrain performances, even reducing vehicle stability. The same process is made with rear axle controller coefficients.

Rear axle control scheme is shown in Figure 46:

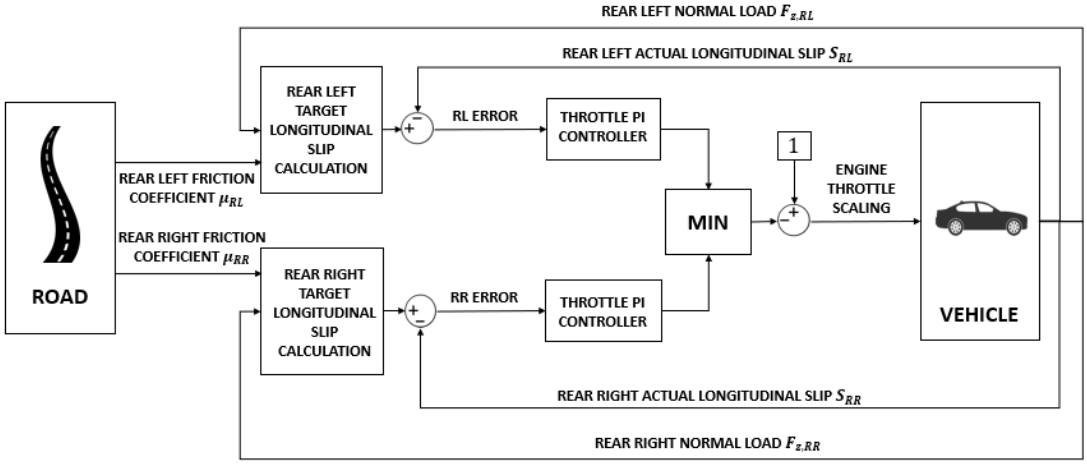

Figure 46: Sport mode rear wheels control scheme

For this driving mode, the opposite choice of *Comfort* one is made: engine throttle scaling signal takes as input the minimum between left and right controllers' outputs. This means that the control activates when both the two wheels are exceeding longitudinal slip limits, and considers as reference the one with lower slip difference with respect to the corresponding threshold. As a consequence, the control acts referring to the wheel with more traction, obtaining the maximum longitudinal acceleration.

On the other side, this control action could generate a not negligible difference between wheels ground longitudinal forces: in case of different road friction, the traction wheel would develop maximum longitudinal force, while the spinning wheel would produce a significantly lower one. In order to balance the yawing moment resulting from this condition, further control is added to the front wheels, as illustrated in Figure 47:

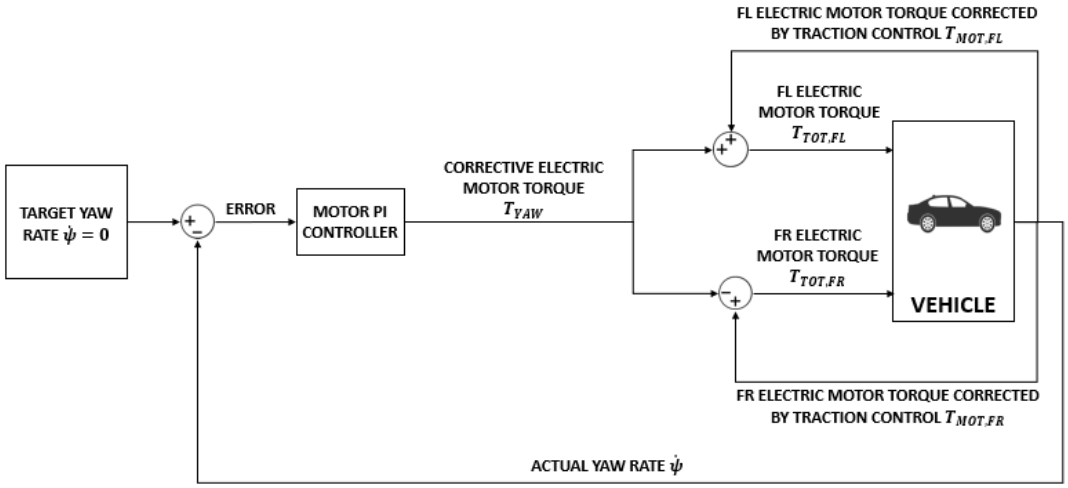

Figure 47: Sport mode yaw-rate control for front wheels

The vehicle yaw-rate is the control variable: when the vehicle is travelling in a longitudinal direction, its target value corresponds to 0 deg/s. If its actual value is different, due for instance to the activation of rear axle slips control, the error is elaborated by a PID controller and leads to an additional corrective electric motor torque. This torque value is added on one front wheel and subtracted to the other, exploiting the possibility to control the two motors independently, in order to achieve a counterbalancing yawing moment and reduce the yaw-rate. In case of the Traction Control and the yaw-rate control activate in the same time on the front wheels, the first one has the priority: it is possible to add a positive torque to a wheel as long as the wheel rotational velocity is lower than the target longitudinal slip corresponding value.

4.2.4 *Wet* mode

If the driver selects *Wet* driving mode, it is supposed that the vehicle is travelling on a wet road, characterized by low friction coefficient, or in general it can be considered a request of a stabler and safer vehicle behaviour.

To reach these targets, *Wet* mode Traction Control scheme considers an algorithm similar to *Comfort* mode: in this way all vehicle wheels are controlled, ensuring vehicle stability. This mode is distinct from *Comfort* one by the fact that "target longitudinal slip calculation" block takes as input road friction coefficient a constant value equal to 0.4. It follows that, independently to the real road

conditions, the control will act as if all the wheels are rotating on a wet surface: target longitudinal slip value is reduced, and the control action would result more restrictive. In addition, PID controllers' coefficients are tuned in order to obtain a faster control reaction in case of activation.

Wet mode control schemes of each front wheel and rear axle are described respectively in Figure 48 and Figure 49:

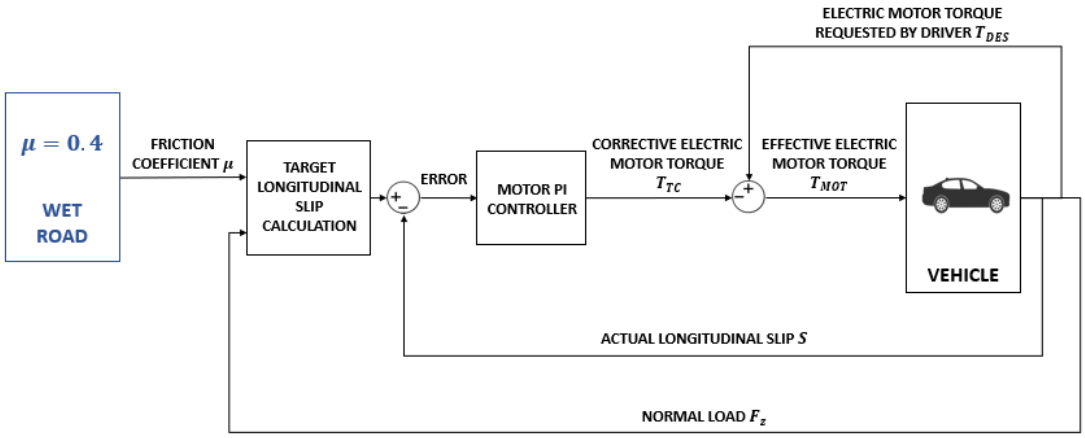

Figure 48: Wet mode front wheels control scheme

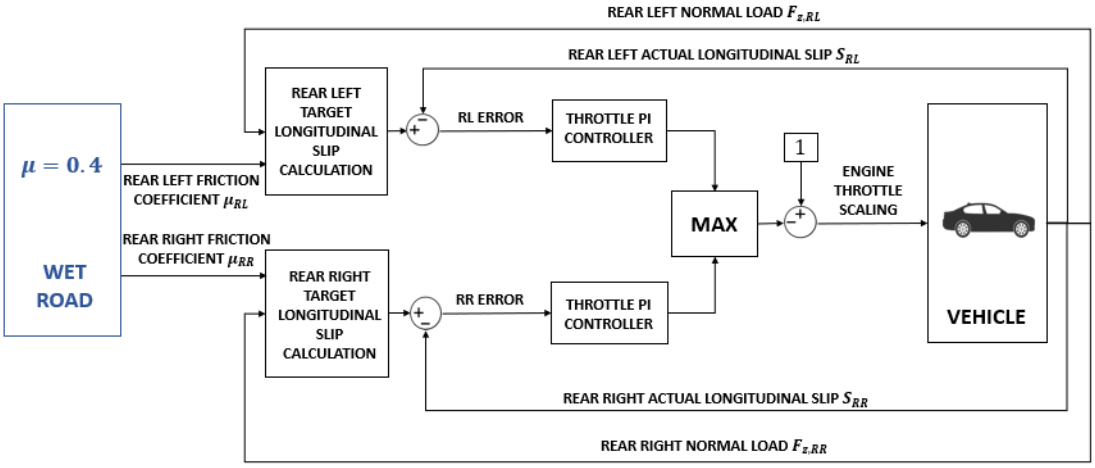

Figure 49: Wet mode rear wheels control scheme

4.3 PID Controller

Engine and motors torque regulations are based on PID controllers: for each wheel, the controller takes as input the error between the desired instantaneous longitudinal slip and the actual one.

PID controller represents a simple implementation of feedback [33]: its algorithm can be described by (4.2):

$$u(t) = K_P\left(e(t) + \frac{1}{T_I}\int_0^t e(\tau)d\tau + T_D\frac{de(t)}{dt}\right) \qquad (4.2)$$

Where u is the control output and e is the control error, which consists in the difference between the setpoint and the process variable; K_P, T_I and T_D are the proportional gain, the integral time and the derivative time respectively. The block diagram of a process with a PID feedback controller is shown in Figure 50:

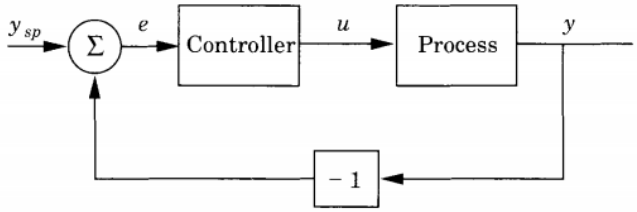

Figure 50: Block diagram of a process with a feedback controller [33]

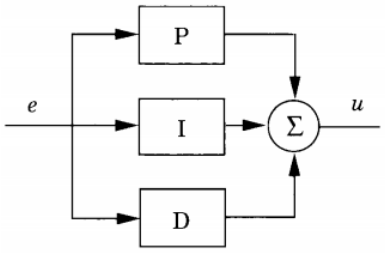

Figure 51: PID controller structure [33]

The corresponding controller transfer function is reported in (4.3):

$$G(s) = K_P\left(1 + \frac{1}{T_I s} + T_D s\right) \qquad (4.3)$$

A complete PID controller includes three terms [33]:

- a proportional action: the control output is proportional to the control error, through the constant K_P; there is always a steady-state error with a pure proportional control: increasing gain value, the magnitude of the error reduces while the control behaviour becomes more unstable;
- an integral action: the control output is proportional to the time integral of the control error, hence based on its past; the presence of an integral contribute in control ensures a null steady-state error: with a finite integral

time T_I value, control response always reach the setpoint; increasing its value, maintaining constant the proportional gain, the control response is faster but more unstable;

- a derivative action: the control output is proportional to the time derivative of the control error, anticipating its future behaviour; it is used to improve the controller stability, selecting the proper value of the derivative time T_D.

PID controller is widely used in industrial plants: process control, motor drives, magnetic and optic memories, automotive, flight control, instrumentation. [31]; its simple structure leads to fast speed calculation, allowing real-time control, and it assures convenient realization and stable and reliable operation [8]. It is also very useful when it is difficult to define a mathematical model of the plant, due to its complexity, and an analytical or computational approach cannot be used for design [32]. Actually, PID controllers are based on microprocessors, which allow to exploit additional features like automatic tuning, gain scheduling and continuous adaptation [33].

The design procedure of a PID controller, which includes the choice of controller structure, should achieve the desired specifications taking into account the limitations in computational power and control signal, based on the available process knowledge [31].

The tuning of PID controller consists substantially in the regulation of gains values in order to obtain the desired performance in terms of attenuation of load disturbances, sensitivity to measurement noise, robustness to model uncertainty, setpoint following [32]. For this purpose, some criteria can be defined to assess the quality of the control action, generally regarding controller time or frequency response [33].

4.4 Control implementation on *MATLAB-Simulink*

The control structure described in the previous paragraphs is implemented on *MATLAB-Simulink*; the overall control scheme is shown in Figure 52:

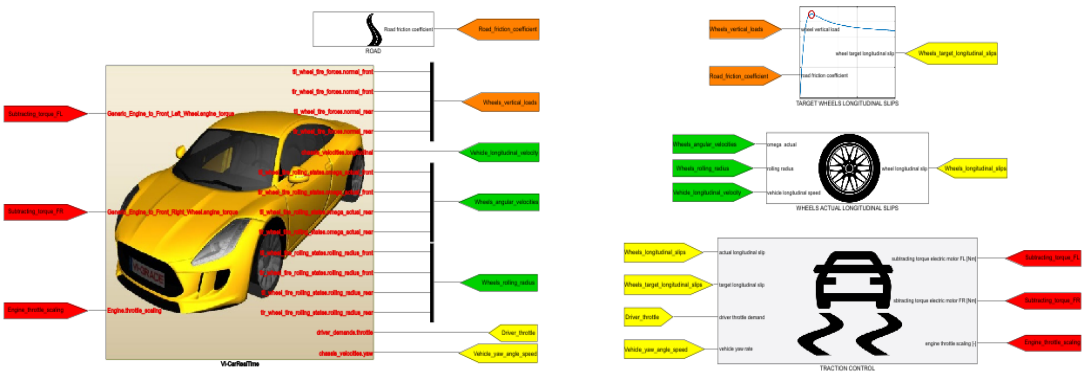

Figure 52: Control scheme on MATLAB-Simulink

Apart from the *VI-CarRealTime* vehicle model block, the control consists into three main blocks: “target wheels longitudinal slip” calculation block, “wheels actual longitudinal slip” calculation block, “traction control” block. In this paragraph, each of them would be illustrated.

The block dedicated to the target longitudinal slip calculation takes as inputs for each wheel the vertical load, from vehicle model block, and the road friction coefficient, which is the output of the road block. For this study, the information about road adherence is directly defined depending to the kind of test that the vehicle would perform: its value can be constant or change with the distance travelled by the vehicle during the manoeuvre. Considering to implement the present control logic on a real vehicle, road friction value would be provided by a proper estimator.

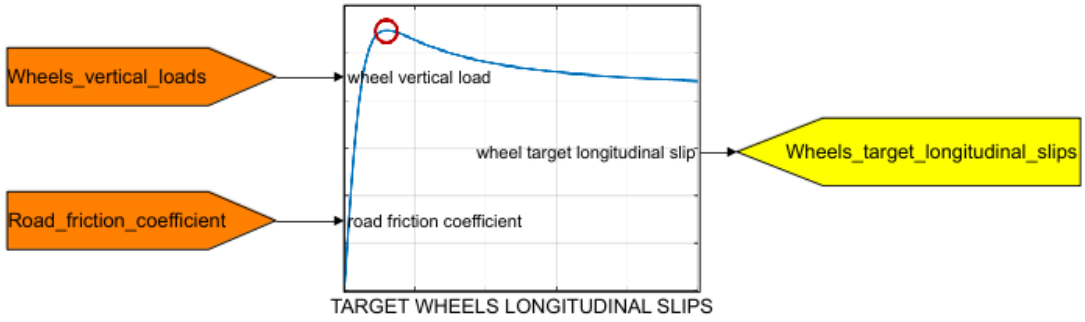

Figure 53: Target wheels longitudinal slips block

The output target value is obtained through a 2D look-up table: the road friction coefficient is always a value between 0 and 1, and the vertical load can take values included in a limited range. For this reason, it is possible to develop off-line maps that can be used for this purpose: for each combination of the input parameters

values, maximum force slip is calculated, using the known tires coefficients, and the table is generated. This choice is also useful in terms of computational effort, which is much reduced if compared, for instance, with a *MATLAB function* block: Pacejka model includes a high number of parameters, hence implementing a function that, at each acquisition time step, repeats the evaluation of longitudinal force curve and searches the slip value corresponding to the maximum would not be functional for an on-line application.

The actual longitudinal slips are calculated from vehicle's longitudinal velocity, wheels angular speeds and wheels rolling radius, that are vehicle model block outputs, through the relationship explained in the equation (2.39):

Figure 54: Wheels actual longitudinal slips block

The controller block takes as inputs: from the previous blocks, the output slips values, in order to compare, for each wheel, the actual and the target one; from vehicle model, the driver throttle demand, useful to activate the controller action, and the yaw-rate, used in *Sport* mode control. Controller outputs are front electric motors subtracting torques and engine throttle scaling, obtained as explained in Paragraph 4.2, that are sent to vehicle model block as inputs:

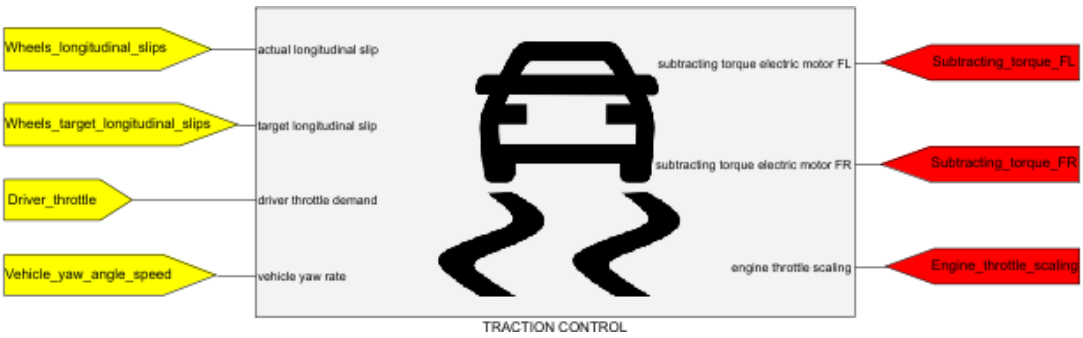

Figure 55: Traction Control block

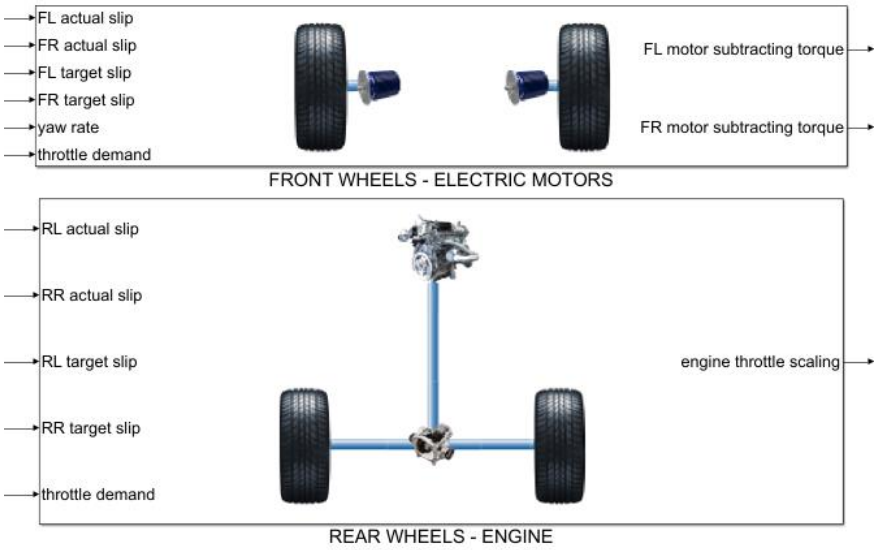

Figure 56: Traction Control sub-blocks

In traction control sub-blocks, trigger signals are implemented in order to established when the control is activated on front left motor, front right motor and engine. When the trigger signal is equal to 1, thus the control is activated, the PID controller of each wheel takes as input the difference between wheel's actual slip and corresponding target slip. Otherwise, PID input is represented by a constant 0 value signal, and the possible integral contribute due to a previous activation is reset. As regards rear axle "engine throttle scaling" signal, it takes the maximum value between left and right wheels PID outputs for *Comfort* and *Wet* modes, while it considers the minimum one for *Sport* mode.

5 Simulation tests results

The designed Traction Control System is validated through several test manoeuvres implemented in the *VI-CarRealTime* simulation environment. In particular, it is possible to define customized *VI-Driver* files through the tool *VI-EventBuilder*: the user can settle driver commands assigning input signal directly to throttle, brake and steering or imposing conditions about vehicle path, velocity, and acceleration during the manoeuvre time.

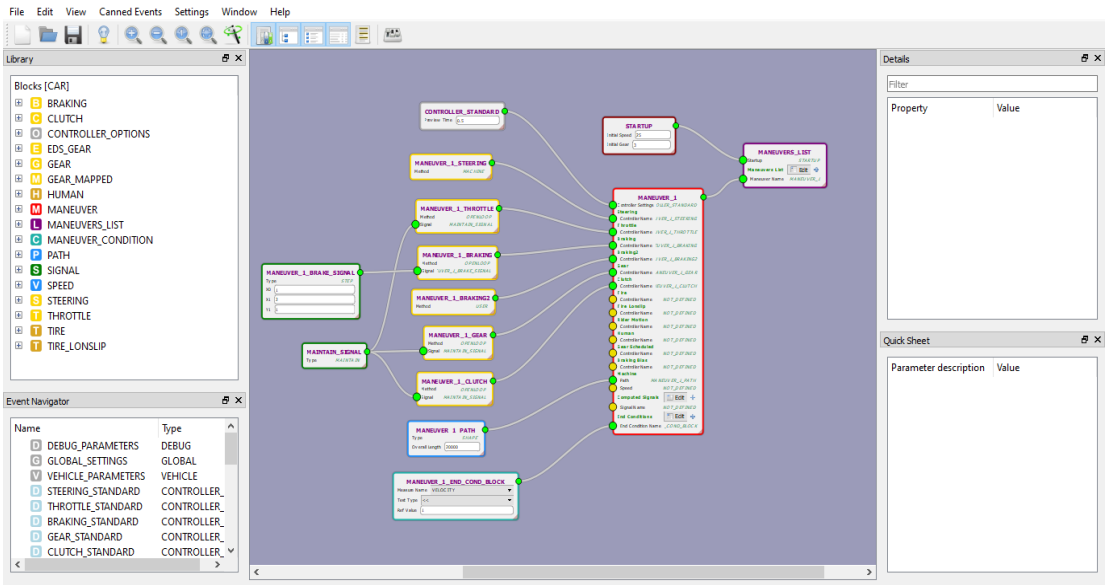

Figure 57: VI-EventBuilder interface

Road characteristics, like width, curvature, height, and friction, can be specified in the *VI-Road* tool creating a *Road Data* file, which consists of a road geometry model. In *VI-CarRealTime TestMode,* the whole event can be created and run, coupling the *VI-Driver* file with the *Road Data* file in a *FileDriven* kind of event.

5.1 Tests scenario

Designed TCS performance is verified through straight-line full-throttle accelerations tests: starting from a speed of 30 km/h, the driver applies an acceleration demand step to 100 % in 0.5 seconds, in order to generate the maximum engine and motors torque.

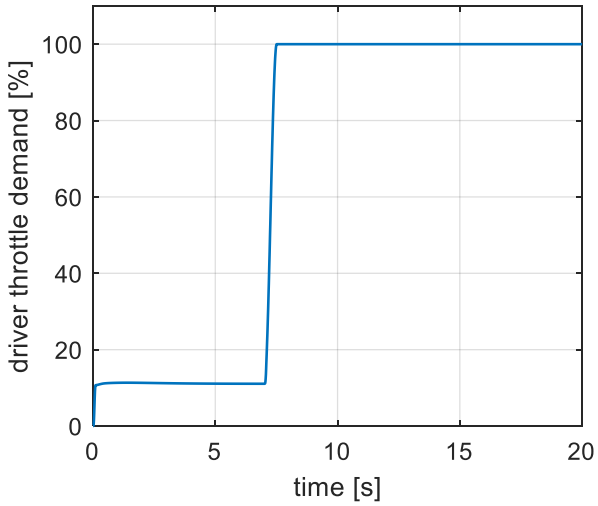

Figure 58: Driver throttle demand during acceleration manoeuvre

The manoeuvre is carried out on three different road conditions:

- ***Mu-split:*** a mu-split road surface is characterized by different adhesion coefficient on the right and left side. On this kind of road, a vehicle without TCS would lose its stability during acceleration because of the different traction of wheels on the two vehicle's sides. If TCS is active on the vehicle, it should help to maintain the straight-line path without requiring a significant driver effort.

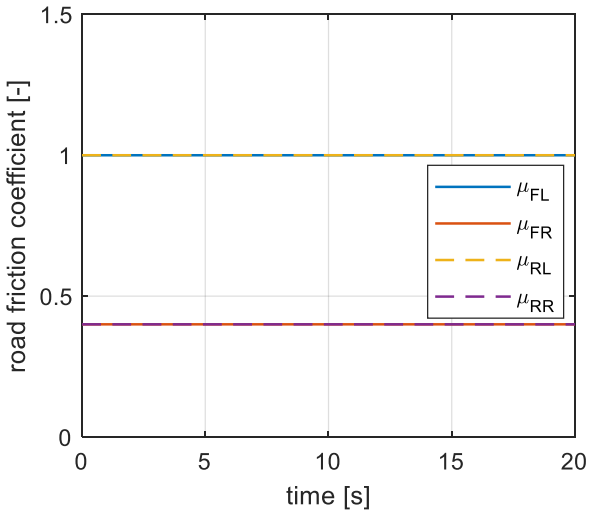

Figure 59: Road friction coefficients during mu-split manoeuvre

- ***Variable Mu-split:*** the road shows different friction coefficients on its two sides, with a variable value during the acceleration: from 1 to 0.5 and then 0.7 for the right side, from 0.4 to 0.8 and then 0.5 for the left one. For this test, a

vehicle behaviour similar to the constant *Mu-split* case is expected, and, in addition, the robustness of control against fast-changing road conditions can be analysed.

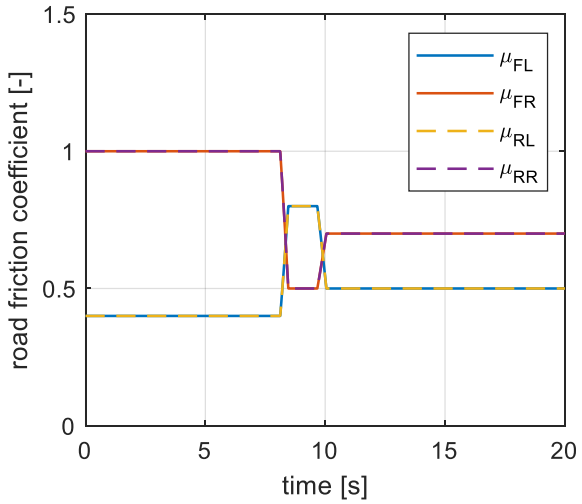

Figure 60: Road friction coefficients on variable mu-split manoeuvre

- ***Low friction:*** the road surface has a uniform low friction coefficient, which reproduces wet conditions. In this case, all the wheels of the passive vehicle lose their adhesion with the road because of their excessive slips; as explained in Paragraph 4.1, this situation represents a dangerous condition because none of the vehicle wheels would be able to generate force the in lateral direction, hence in presence of a steering driver demand the vehicle would react with an unstable behaviour. The TC system attempts to limit each wheel slip, making the most of surface friction and enhancing vehicle traction.

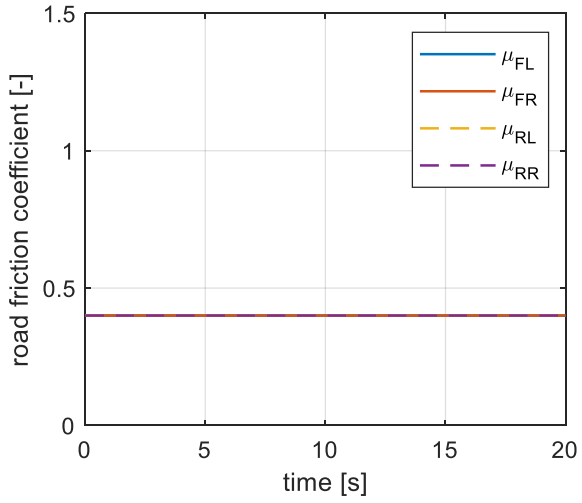

Figure 61: Road friction coefficients during low friction manoeuvre

5.2 Comparison with passive vehicle

The developed algorithm's effectiveness is demonstrated through a comparison between the vehicle equipped with TC and the passive vehicle, performing the simulations of the three described scenarios.

5.2.1 *Mu-split* road

The simulation outputs included in the time range between 7 and 13 seconds, which is involved by the control activation, are reported.

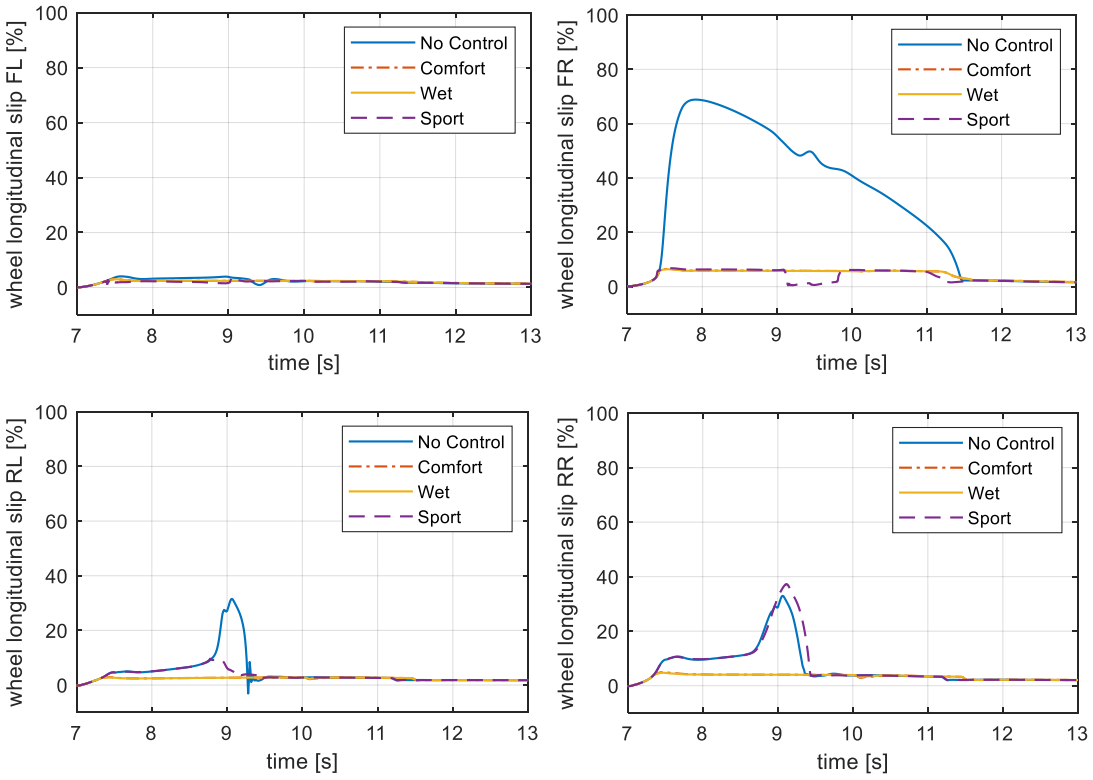

Figure 62: Wheels longitudinal slips during mu-split test

Considering the results shown in Figure 62 after the acceleration command, the rotational speed of passive vehicle right wheels, which are in contact with lower adhesion coefficient, diverges rapidly, as expected. On the rear axle, owing to the LSD differential action, also the left wheel starts to spin: the differential transfers a higher torque to the traction wheel in order to accelerate it, until it reaches the same longitudinal slip value of the right wheel, which receives a lower torque. This condition leads the vehicle to the instability, confirmed by the steering wheel

required to maintain the vehicle straight-line trajectory: it is necessary to balance the yawing moment generated by the different left and right sides longitudinal forces. The simulation driver applies first almost 70 deg in 1.5 seconds and then returns to 0 deg in the opposite steering direction in less than 0.5 seconds: this represents a significant effort not always guaranteed by a real driver.

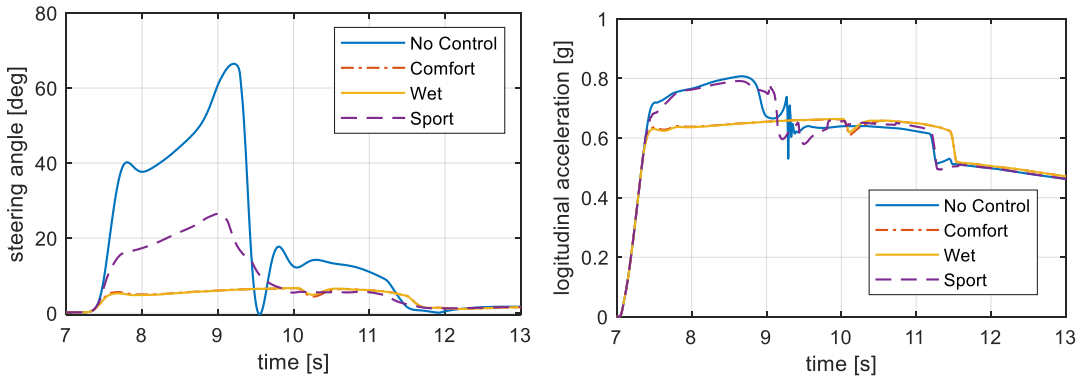

Figure 63: Driver steering angle and vehicle longitudinal acceleration during mu-split test

With the activation of TCS, the vehicle shows overall better behaviour: all the three modes give more stability limiting wheels spinning. Comparing the three control modes, it can be observed that *Sport* one allows the vehicle to reach the maximum longitudinal acceleration performance and, at the same time, requires a steering angle higher than *Comfort* and *Wet* ones, but still much lower than the passive vehicle and with a peak value compatible with a sporty driving. These results represent a consequence of the different actions of TCS on wheels longitudinal slips for each mode.

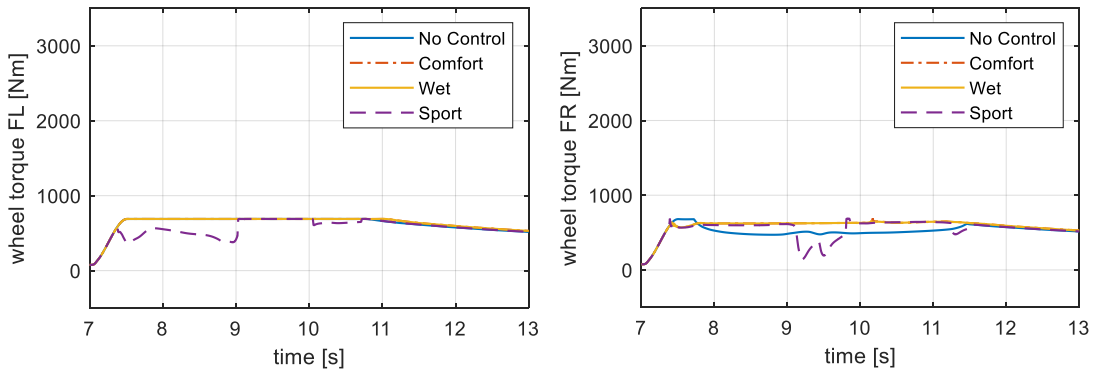

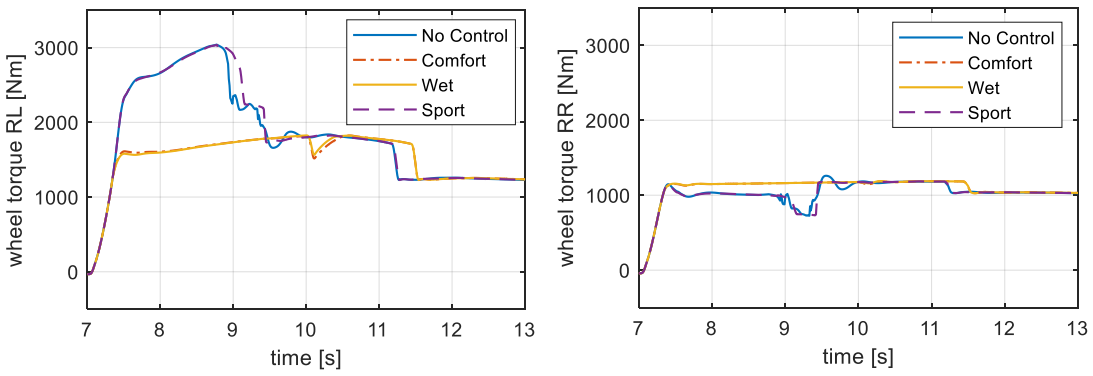

Figure 64: Wheels traction torques during mu-split test

Regarding passive vehicle behaviour, it can be observed from Figure 62 and Figure 64 that, despite higher traction torques are applied on the rear wheels than on the front ones, the first wheel that starts to spin is the front-right one. This result can be explained by the longitudinal load transfer caused by the acceleration.

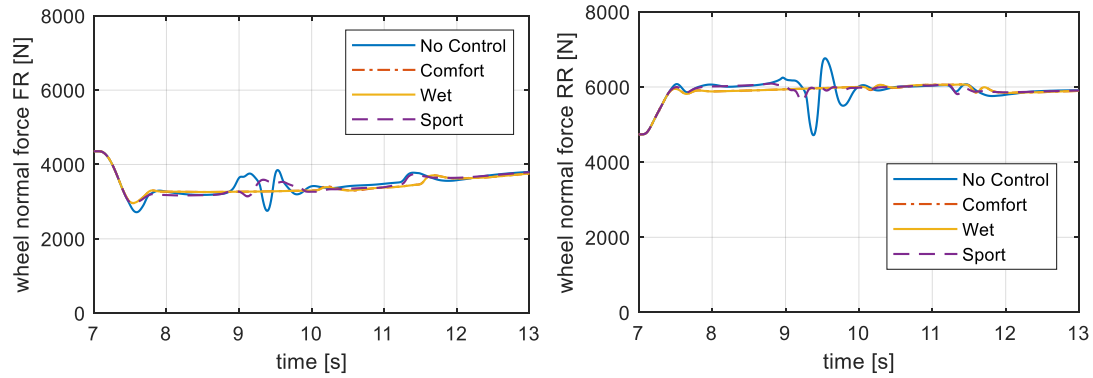

Figure 65: Right wheels normal load during mu-split test

Figure 65 shows the vertical forces on the wheels rotating on the low friction side: during the first seconds of the acceleration, an average difference of 3000 N is generated. Consequently, the adherence of the front-right wheel with the road is damaged, and it starts to spin immediately.

At the rear axle, *Sport* mode adjusts engine torque value referring to the less spinning wheel, which is the left one in the specific case: in this way, a higher longitudinal acceleration value is reached with respect to *Comfort* and *Wet* mode; this result is also achieved thanks to the action of the differential, which still transfers more torque to the traction wheel as a consequence of the difference of slip between left and right side wheels. At front wheels, the electric motor torques

exhibited in Figure 64 result from both longitudinal slips and yaw-rate controls: without the last of them, only the right motor torque would be reduced to regulate the wheel spinning, while, in this case, further subtracting torque contributes can be observed. It is possible to compare driver steering and driver steering speed of *Sport* mode considering the cases of yaw-rate control and no yaw-rate control to verify its performance, as shown in Figure 66:

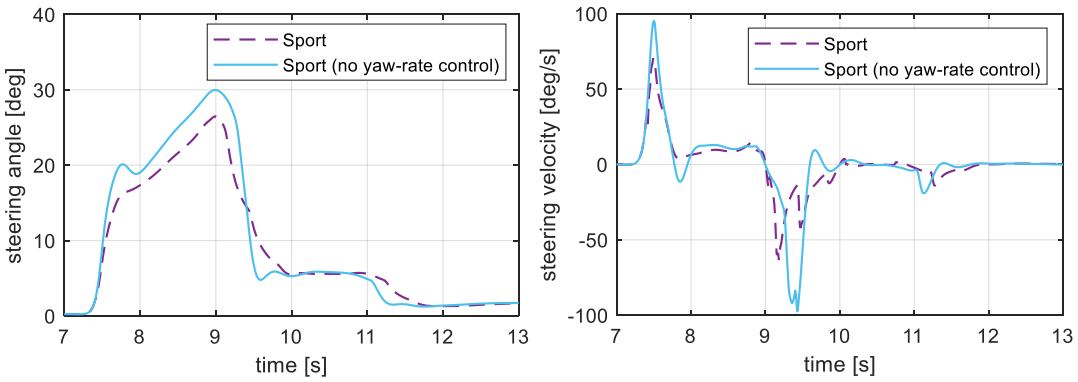

Figure 66: Driver steering angle and driver steering angle speed during mu-split test (Sport mode)

The yaw-rate control presence permits a reduction of the maximum steering angle required to the driver, from 30 deg to 26 deg, and of steering oscillations in general, confirmed by lower peak values of steering velocity.

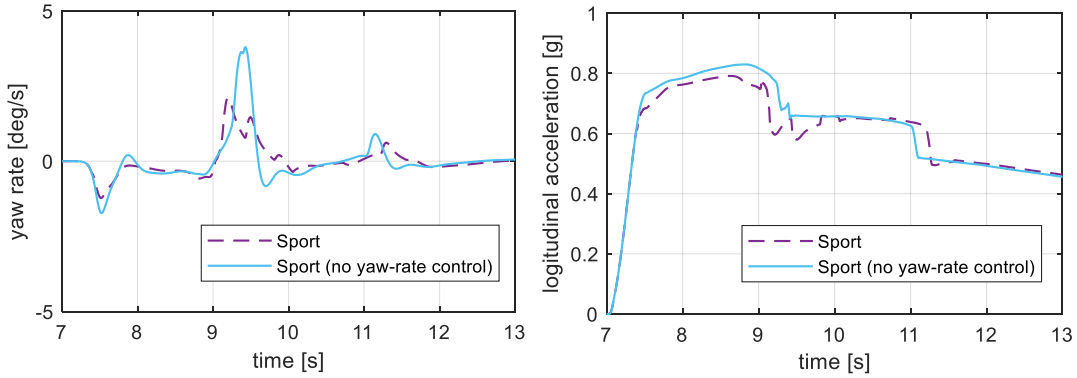

Figure 67: Vehicle yaw-rate and longitudinal acceleration during mu-split test (Sport mode)

Since for this manoeuvre the yaw-rate control activation causes only a reduction of front motors traction torque, it follows that also the overall vehicle longitudinal acceleration is reduced. However, this effect is considered acceptable if compared with the advantages in terms of vehicle stability. Furthermore, it has to be noticed that, during acceleration, the longitudinal load transfer increases the rear axle wheels vertical load; as a result, most of vehicle longitudinal acceleration is due

to the rear axle traction contribution.

As regards *Comfort* and *Wet* modes results, it can be noticed that they show behaviours similar to each other: even if *Wet* mode has a lower threshold value for the left side, since it refers always to $\mu = 0.4$, the wheels for which the control is activated, on both front and rear axles, are the right ones, that are rotating on a low-friction road; as a result, the reference values on the vehicle right side are the same for both the two modes. The fact that vehicle's longitudinal acceleration and driver steering angle reach lower maximum values for *Wet* mode is related to the different PI controllers' coefficients. Regarding the influence of LSD action on the rear axle, the corrective torque distributed by the differential is lower than for the *Sport* mode case, and it is always directed to the left wheel, which shows more traction: for these two modes, the control limits the engine torque referring to the wheel which is spinning more; hence its effect helps in reducing the difference of slip between left and right side.

5.2.2 Variable *Mu-split* road

In the same way of the previous test, the simulation outputs included in the time range between 7 and 13 seconds are reported.

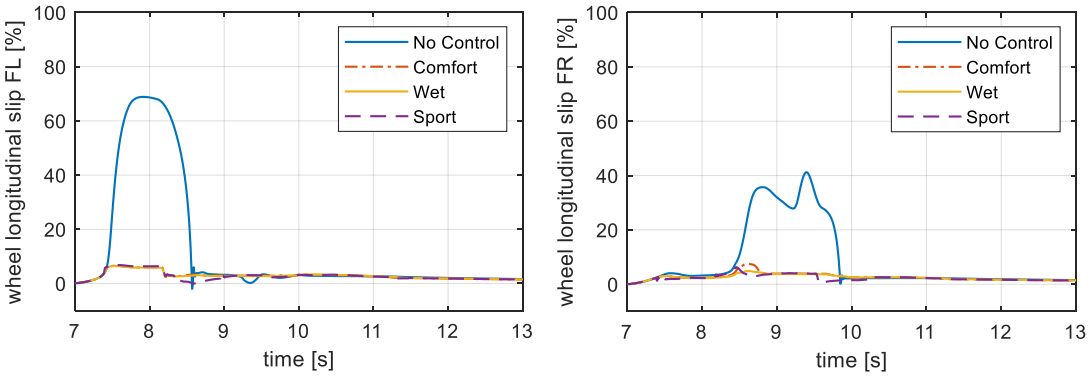

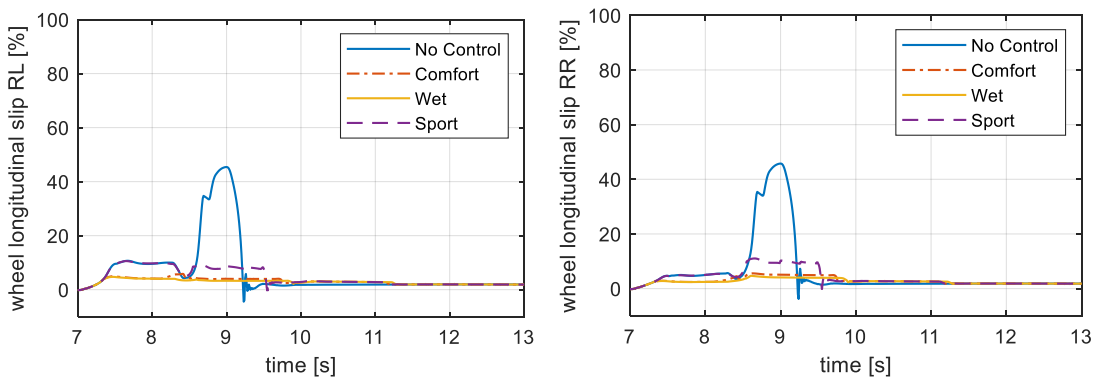

Figure 68: Wheels longitudinal slips during variable mu-split test

In this test, the results are similar to the previous one; a higher instability is expected because the vehicle travels on the road with variable adhesion coefficient on both sides: the rapid change of lower friction road side causes the tires to lose their grips alternatively, developing excessive longitudinal slip values during transition moments. As a consequence, the yawing moment generated on the passive vehicle has a variable sign: the corresponding driver steering wheel angle oscillates rapidly between the two directions, with a maximum amplitude of more than 100 deg in 1 second.

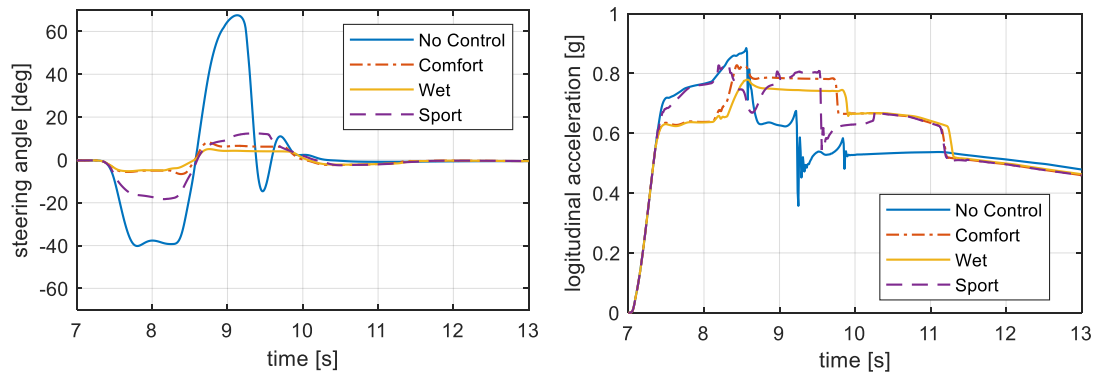

Figure 69: Driver steering angle and vehicle longitudinal acceleration during variable mu-split test

As regards the control effects on vehicle behaviour, *Sport* mode is confirmed to represent the best compromise between the maximum longitudinal acceleration performance and a proper driver steering wheel angle: as shown in Figure 69, during the first part of the manoeuvre the highest acceleration value is reached on *Sport* mode, and the steering angle value is halved with respect to the passive vehicle. When the road friction coefficients change, the yaw-rate control reduces the electric motor torques to increase the vehicle stability; the effects of this control are more evident than in constant mu-split test: the first steering angle

peak value is reduced of almost 10 deg, and then it reaches in the opposite direction 12 deg instead of 15 deg.

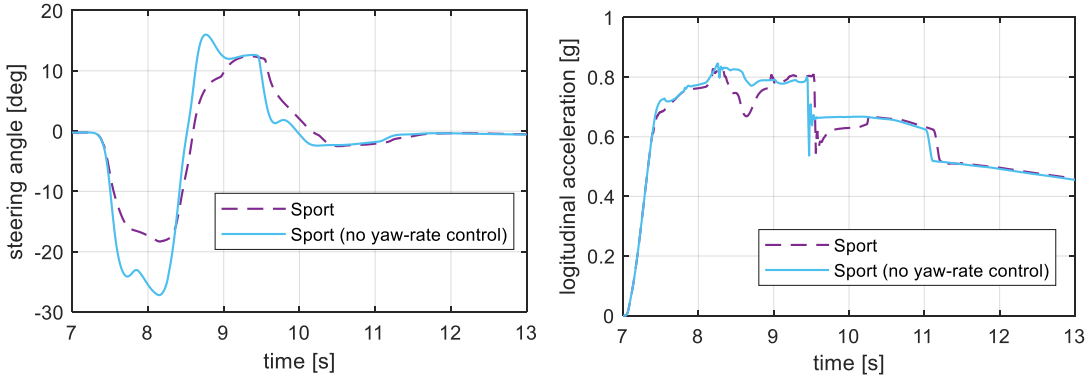

Figure 70: Driver steering angle and vehicle longitudinal acceleration during variable mu-split test (Sport mode)

Unlike the constant *mu-split* test, differences are observed between *Comfort* and *Wet* mode: initially, the control is activated because the left side wheels are spinning, and the reference friction coefficients are the same (equal to 0.4); after the sudden change of μ value, *Comfort* mode considers the effective $\mu = 0.5$ for the calculation of the slip target, while *Wet* takes the default 0.4; hence, in *Wet* mode, the control activation decreases more the traction torques. It follows that for this mode the maximum longitudinal acceleration and driver steering angle are lower than for *Comfort* one, as depicted in Figure 69.

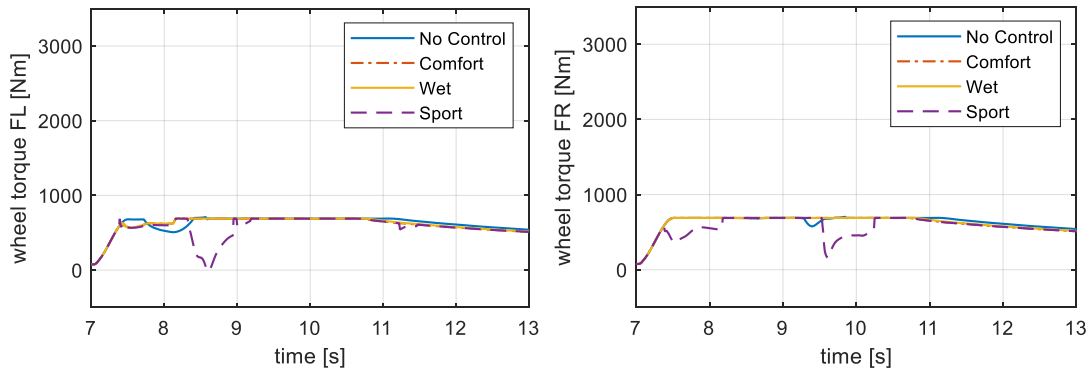

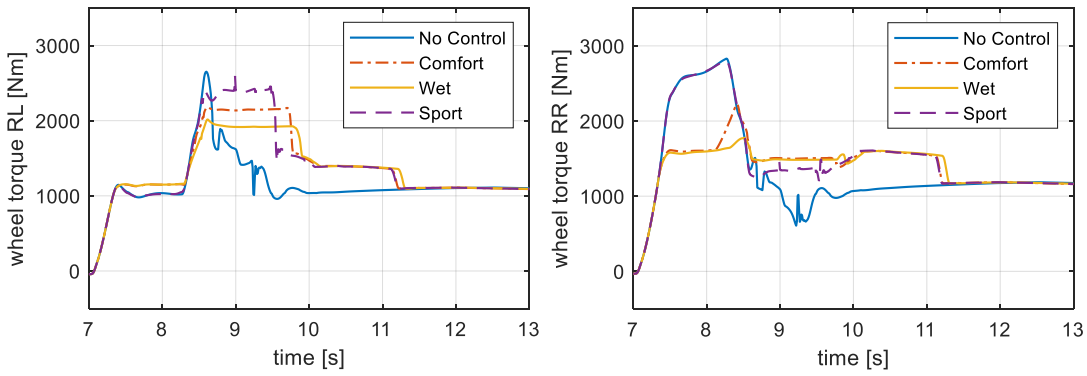

Figure 71: Wheels traction torque during variable mu-split test

5.2.3 Low friction road

During this test, the target road friction value is 0.4 for all the control modes, as a consequence, the results on vehicle behaviour are expected to be differentiated only for the contribute of PI coefficients value. The simulation outputs included in the time range between 7 and 17 seconds are reported.

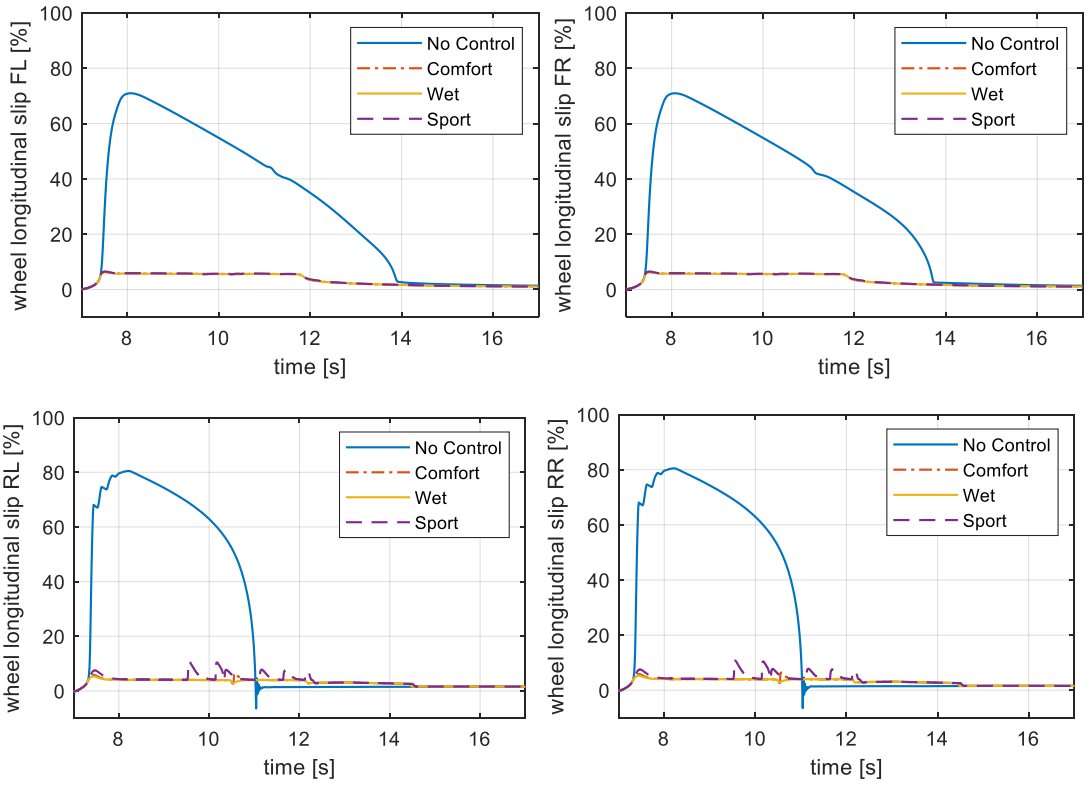

Figure 72: Wheels longitudinal slips during low friction test

As regards the passive vehicle, it can be observed from Figure 72 that all the wheels exceed the limit: the instability due to the loss of adherence requires a

reaction of the driver with a steering command to maintain the trajectory, after a few seconds from the initial acceleration command. With the TC intervention, the driver steering effort is nulled: for each axle, left and right wheels are rotating with the same speed, with small slip values, and are subjected to the same working conditions. On the rear axle, the engine torque reduced by the control is distributed equally by the differential, and the same longitudinal forces are developed on both axle sides; as a result, no yawing moment is generated, and the vehicle maintains the straight-line trajectory.

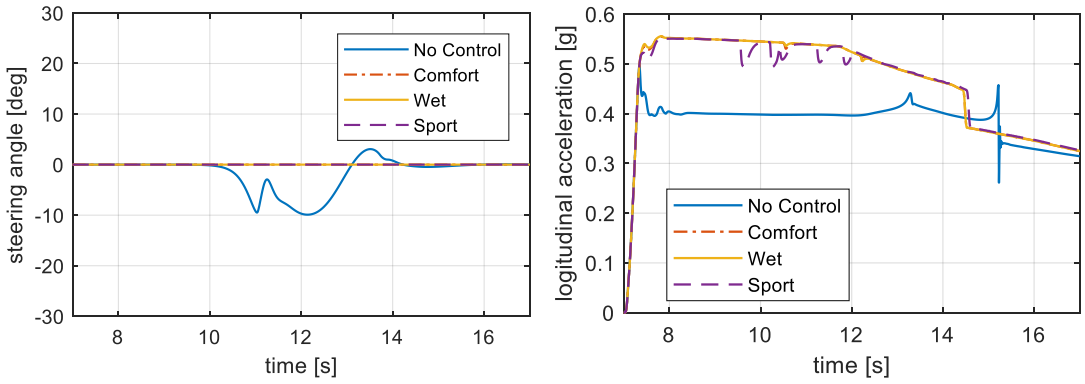

Figure 73: Driver steering angle and vehicle longitudinal acceleration during low friction test

Unlike the *mu-split* tests, it can be observed from Figure 72 that on the passive vehicle all the wheels on the low surface start to spin immediately: during this manoeuvre smaller longitudinal acceleration is reached and the longitudinal load transfer is lower, consequently all the wheels lose quickly the adherence with the road.

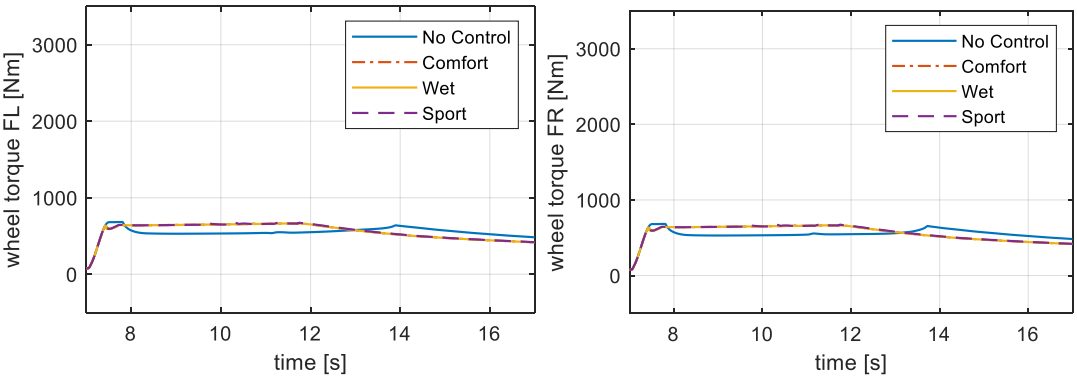

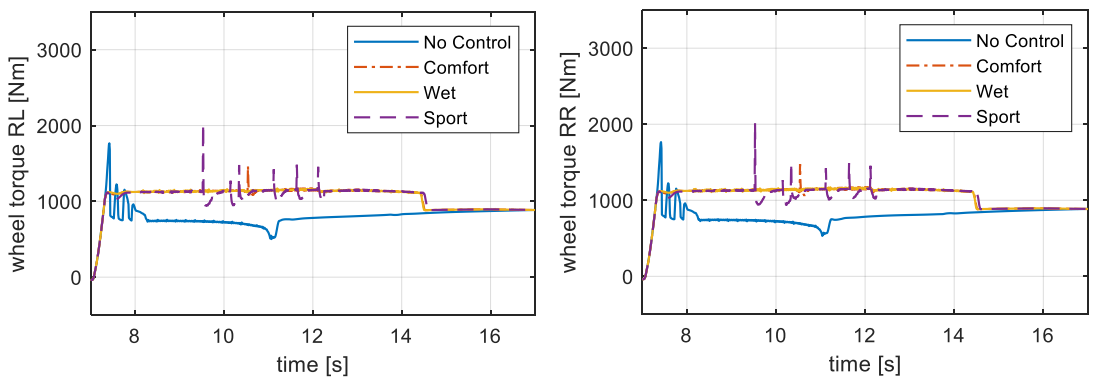

Figure 74: Wheels traction torque during low friction test

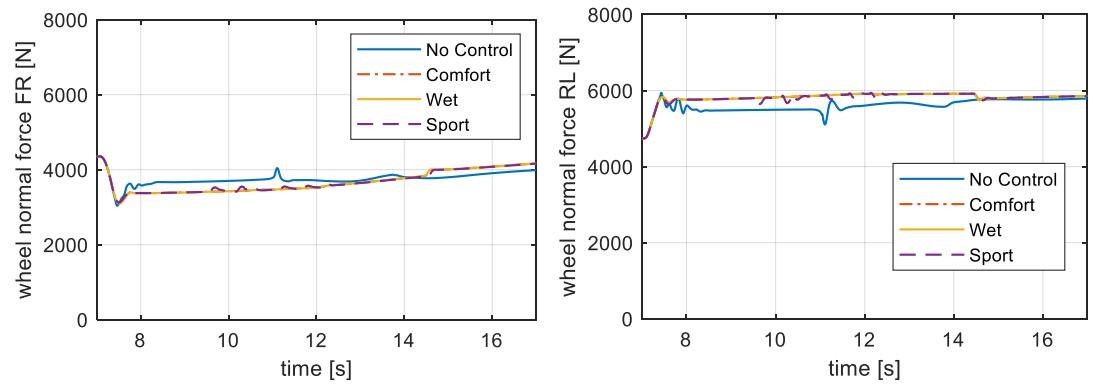

Figure 75: Right wheels normal load during low friction test

It can be observed that for this manoeuvre, which simulates the condition of the wet road, the *Wet* mode guarantees the best traction condition: thanks to the fact that the controller shows an instantaneous effect on the vehicle powertrain when it activates, it is confirmed to be the safest mode, proper for adverse environmental conditions. Moreover, it can be noticed that the value of the instantaneous road friction coefficient taken as input in *Comfort* and *Sport* modes algorithms is detected by an estimator, which is not necessarily accurate in the measurement. Considering, for instance, different estimated μ values, the vehicle behaviour for *Comfort* mode is shown in Figure 76:

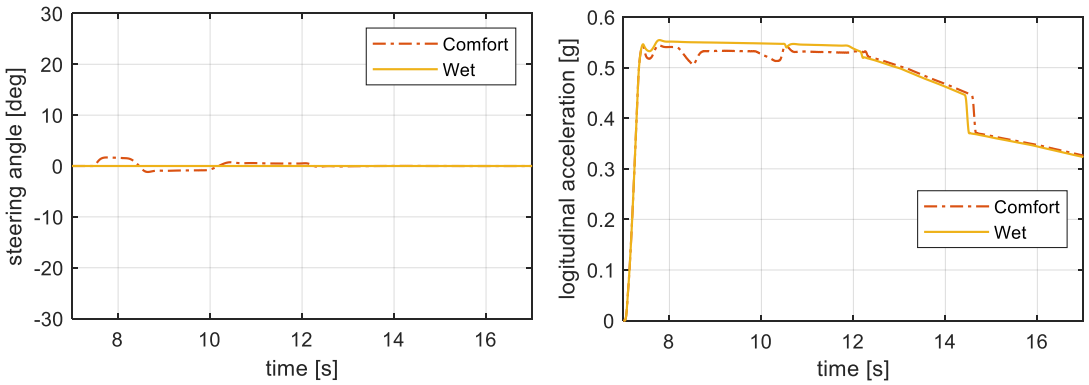

Figure 76: Driver steering angle and vehicle longitudinal acceleration during low friction test (different μ value estimated)

It can be noticed that the driver steering is little affected by this change because the control action, in any case, limits wheel slips under an acceptable value (the worst case corresponds to a measured friction value of 1). The maximum longitudinal acceleration value is reduced, corresponding to a loss of traction which can represent a problem for the wheel's reduced capability to generate forces in lateral direction.

5.3 Comparison with internal *VI-CarRealTime* TC system

In the *VI-CarRealTime* environment it is possible to activate an embedded TCS, which acts on the effective motors' throttle demand. When the vehicle's wheel starts to spin exceeding the longitudinal slip threshold, the throttle command on the respective motor is reduced with a proportional gain. It is possible to regulate the TCS action settling for each vehicle's motor the longitudinal slip threshold value and control's proportional gain in the powertrain subsystem properties.

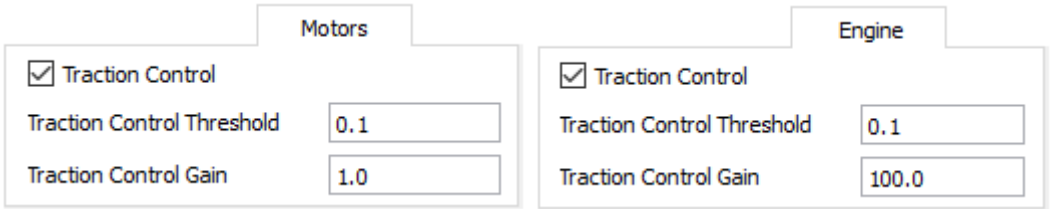

Figure 77: VI-CarRealTime TCS options for electric motor and engine

It is interesting to make a performance comparison between this TC, which has a fixed target value independent from the instantaneous wheels' vertical loads and

friction coefficients, and the *Comfort* and *Sport* modes of the proposed control method.

The first test considered is the acceleration on constant *mu-split* road described in Paragraph 5.2.1: the simulation outputs are reported in Figure 78.

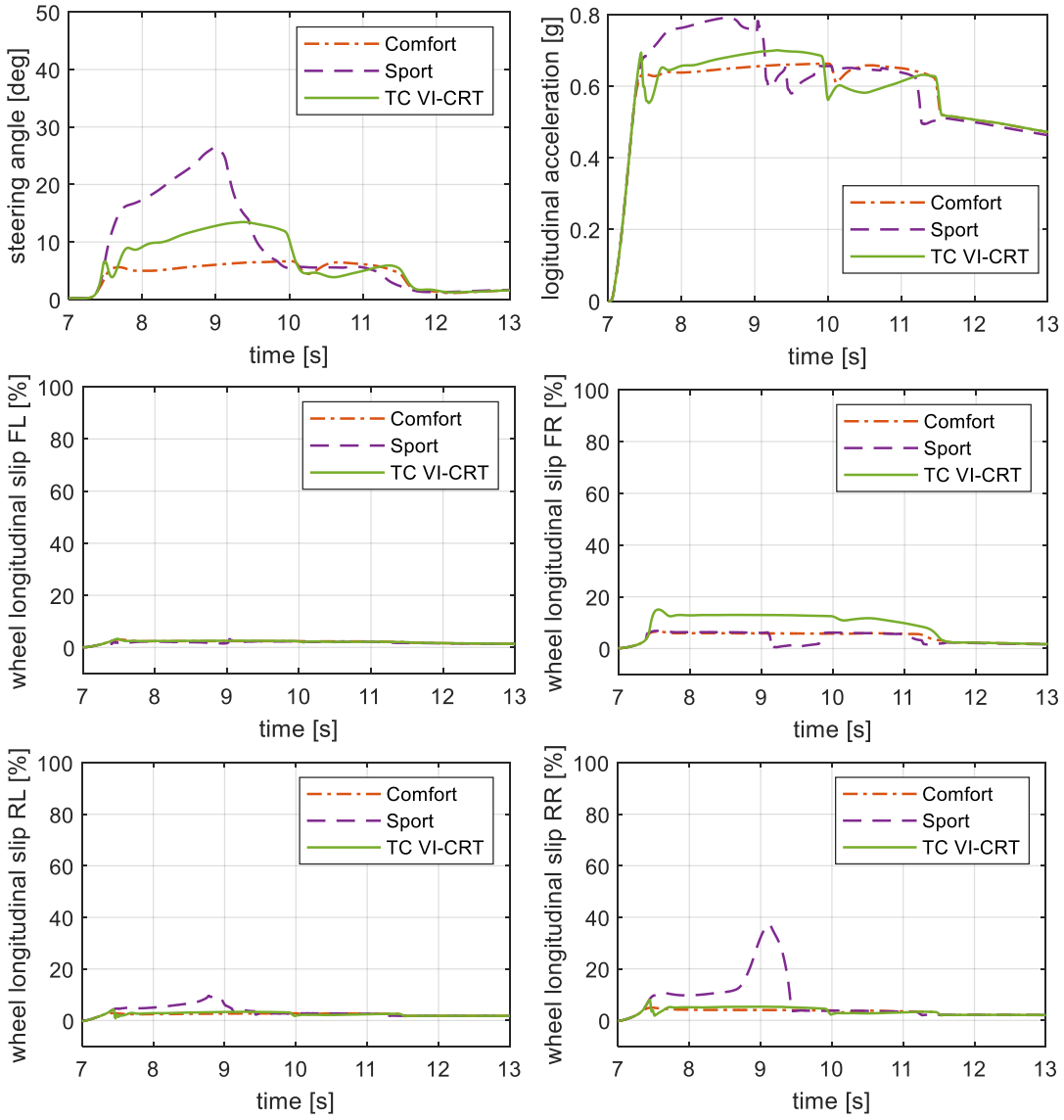

Figure 78: Comparison of designed TC (Comfort and Sport modes) and VI-CRT TC on mu-split test: driver steering angle, longitudinal acceleration, wheels longitudinal slips

It can be observed that the results of *VI-CRT* control are a middle ground between the *Comfort* mode vehicle behaviour and the *Sport* mode one. The vehicle reaches higher longitudinal acceleration than *Comfort* mode, but not the maximum possible value. On FR wheel, the *VI-CRT* target is higher than the value at which the tire generates the maximum longitudinal ground force because the control is

not optimized; hence it has less traction. At the rear axle, the wheels are slowed down more than is needed to make the most of the left side traction, represented by *Sport* mode. The control based on a not optimized target causes a higher driver steering demand than *Comfort*, with a maximum of 13 deg.

The same conclusions can be obtained for the variable mu-split test; thus the second shown comparison is the acceleration on the low friction road, described in Paragraph 5.2.3, whose results are shown in Figure 79.

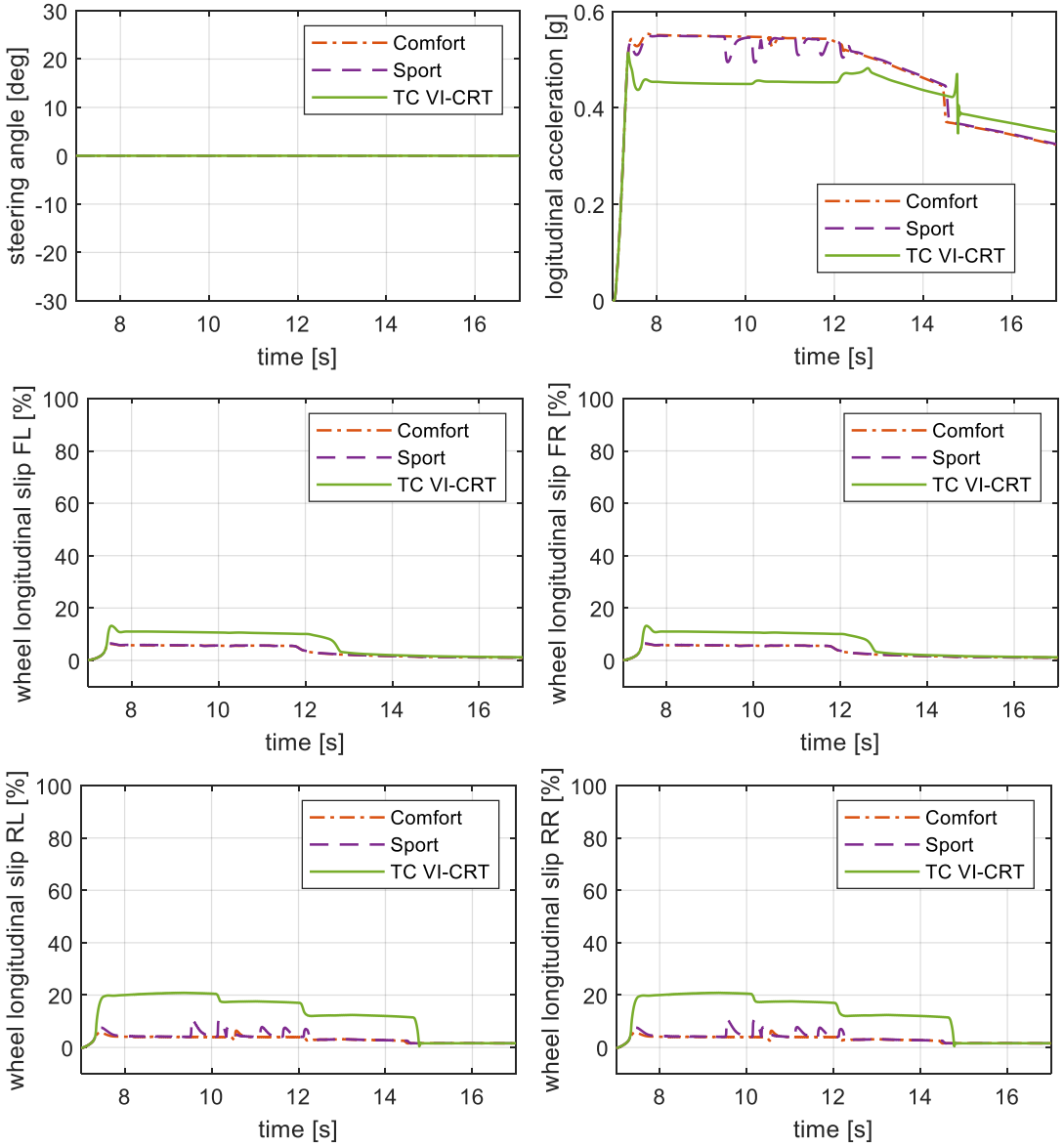

Figure 79: Comparison of designed TC (Comfort and Sport modes) and VI-CRT TC on low friction test: driver steering angle, longitudinal acceleration, wheels longitudinal slips

In this case, the *VI-CRT* control target value is higher than the designed TC one during all the manoeuvre; consequently, the wheels spinning is higher than in

Comfort and *Sport* modes both, and the vehicle loses traction. On the straight-line manoeuvre, there is no evidence of vehicle instability because the *VI-CRT* control still limits wheels slips, and the wheels of the same axle rotate at the same speed hence no yawing moment is generated; however, this condition can represent a problem in case of request of wheel lateral ground forces.

6 Driving Simulator results

The three control modes are tested on a dynamic driving simulator: the same vehicle model used for *VI-CarRealTime* off-line simulations is implemented on the simulator system, and comparisons between passive and active vehicles can be made in terms of driver feeling.

The simulator is called *dynamic* since it is characterized by a motion system that provides accurate feedback to the driver about vehicle handling and ride behaviour. For this work, in particular, the tests are carried on the Danisi Engineering dynamic simulator, provided by VI-Grade, which is equipped with a nine-degrees-of-freedom moving platform, called *Driver in Motion* (*DiM*) [34].

Figure 80: Danisi Engineering dynamic driving simulator [35]

In addition to precise motion perception, the real driving situation feeling is also given by the virtual environment surrounding the simulator. First of all, the driver sits in a real cabin taken from a vehicle, and a virtual road scene is projected on a screen all around him: the visual system is necessary to give the driver the correct impression about vehicle speed and movement. To obtain a realistic driver interaction with commands, the simulator cockpit is equipped with additional actuators that imitate faithfully the feel of pedal and steering wheel. Engine and driving noises are also reproduced, depending on engine

power, engine speed, and driving speed, to let the driver perceive the external environment as realistically as possible [36].

Using driving simulator tests leads to many advantages: it permits to identify problems earlier in the design process [34], and to correct them reducing systems' development times and costs. With respect to road tests, driving simulator ones guarantee: no risks for the driver and the environment, allowing a safe representation of critical driving situations; the possibility to repeat the same test with identical conditions many times, showing high reproducibility; quick and simple changes of vehicle and environment (tracks, weather conditions) parameters [36]. For this study, the dynamic driving simulator is exploited to assess the designed TC system's effectiveness reproducing the same road scenarios analysed in Paragraph 5.1.

6.1 Tests executions

Before starting tests executions, it is necessary to let the driving simulator system communicate with the control logic designed on *Simulink*. First of all, the *VI-CarRealTime* vehicle model is implemented on the simulator to obtain the same handling and ride dynamic responses of off-line tests. Then, road scenarios are created: infinite straight-line roads with high friction ($\mu = 1$), low friction ($\mu = 0.4$) and mu-split ($\mu_{left} = 1, \mu_{right} = 0.4$) surface respectively.

The *Simulink* scheme is rearranged to be compatible with the simulator: the vehicle model block is substituted by more blocks, each of them representing the corresponding input or output simulator channel. The new scheme is then compiled and then uploaded on the system. Regarding the electric motors, the acquisition of the subtractive torques, generated by the control in case of activation, have to be specified to the system before starting the tests.

After setting all these initial aspects, the maximum acceleration performances are executed. The first test is made on a mu-split surface: starting from 30 km/h, the driver imposes a 100 % throttle step demand and tries to maintain the straight-line trajectory. The same manoeuvre is repeated with the passive vehicle and the

active one, considering each control mode.

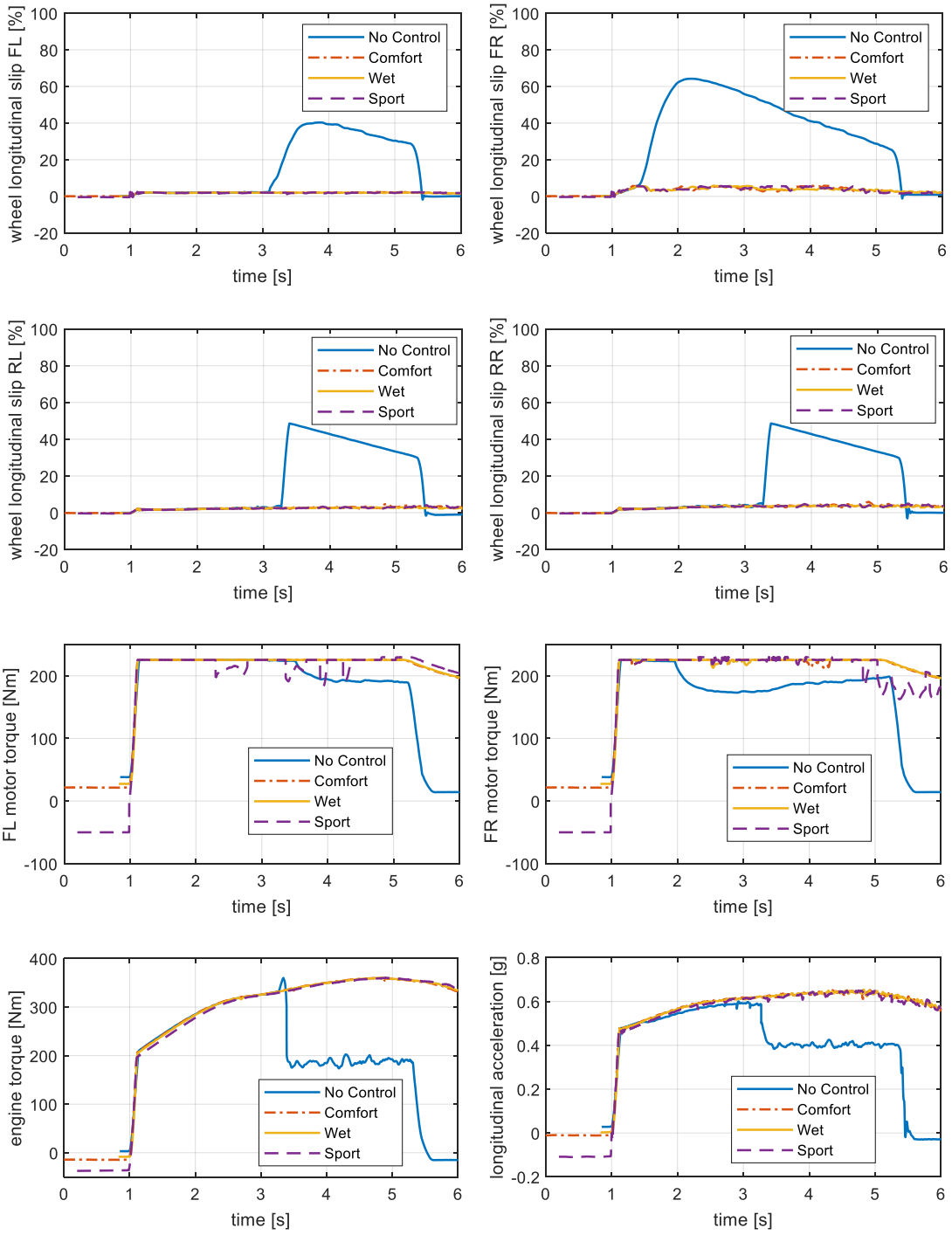

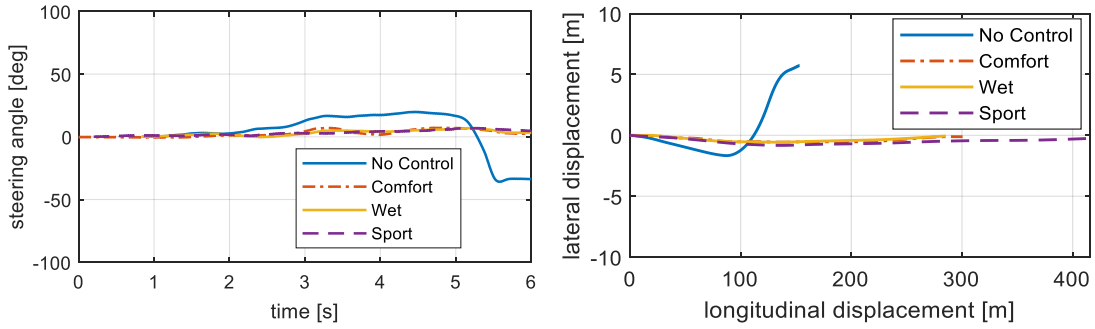

Figure 81: Results of mu-split manoeuvre: wheel longitudinal slips, motors and engine torque, vehicle longitudinal acceleration, driver steering angle, vehicle trajectory

As shown in Figure 81, the driver steering reaction is not sufficient to maintain vehicle control and guarantee the straight-line trajectory on the passive vehicle. Initially, only the front-right wheel starts to rotate excessively, due to the significant longitudinal load transfer during the acceleration, as explained for off-line performance. The driver does not immediately perceive the loss of adherence on the right side of the vehicle, but after a few moments, when the vehicle has already lost its stability. This unstable condition does not permit to reach good acceleration performance. Instead, as can be seen by the trajectory plot, the vehicle goes on the right side of the road: this also causes the front-left wheel's spinning, changing from high to low friction surface.

With the control activation, the vehicle shows higher stability. It reaches higher longitudinal values and maintains the straight-line trajectory with a small driver steering effort: the required steering angle maximum value is lower than 10 deg for all the three modes.

Unlike the corresponding off-line test, there are no significant differences between *Sport* mode and the other two ones. In the first part of the acceleration, only the front-right wheel causes the control activation; hence the vehicle response is similar for each control mode. When also the rear axle wheels spin, the Sport modes provide a slightly higher engine torque. During all the duration of the manoeuvre, *Sport* mode acceleration performance is penalized by the yaw-rate control, which reduces the torque of front-left and front-right motor alternatively. Consequently, it can be affirmed that the vehicle behaviour seems to be substantially the same for all the three control modes in a simulation of the

real driving condition of this scenario.

The second tested manoeuvre is the maximum straight-line acceleration on the low friction surface. Also in this case, the vehicle behaviour with and without control is observed.

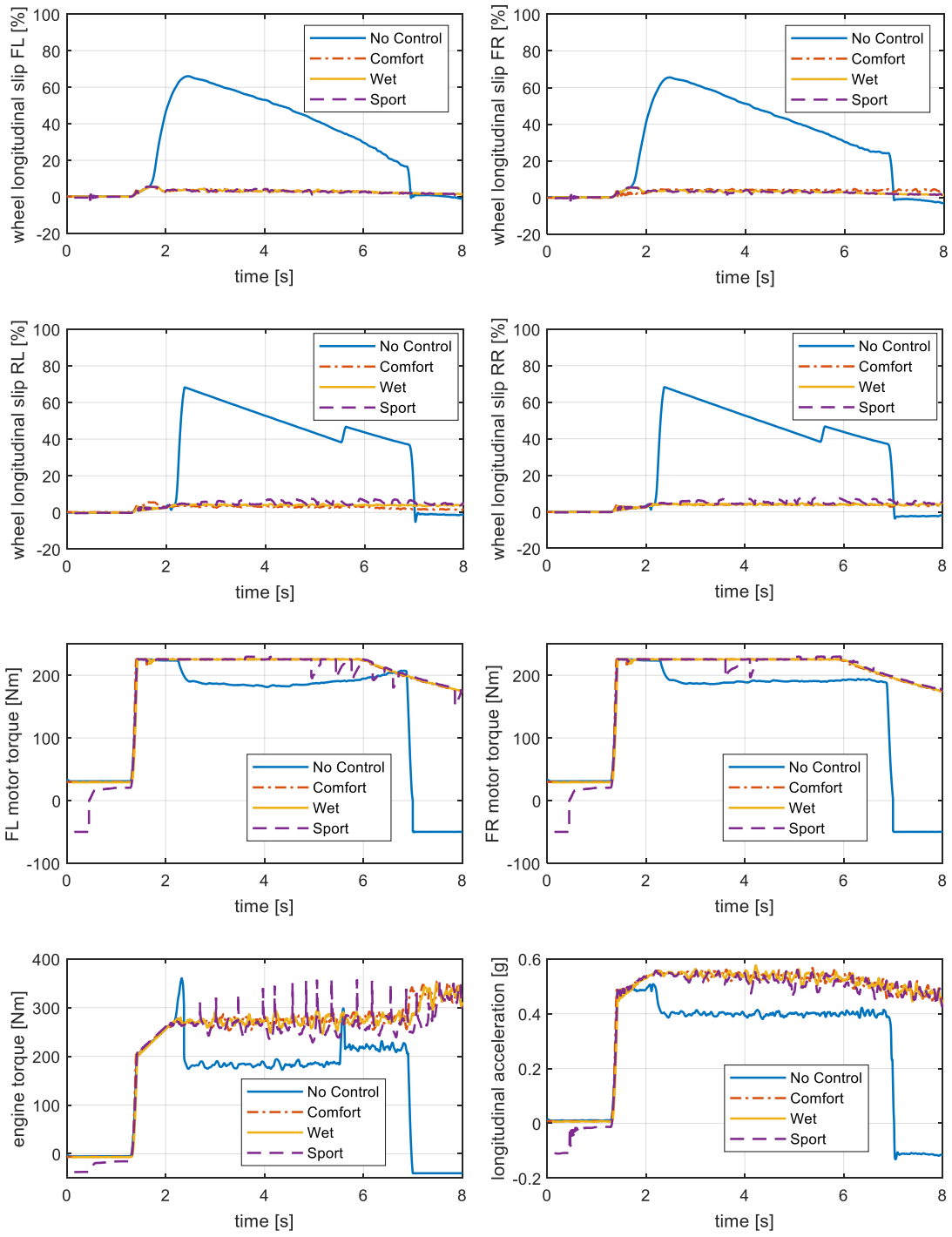

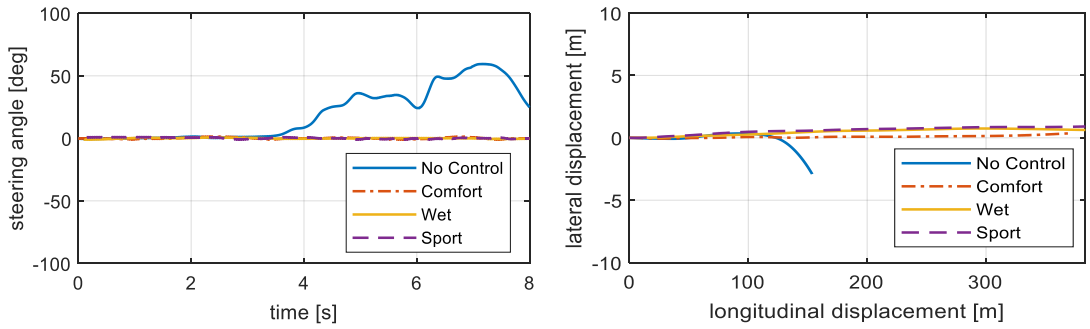

Figure 82: Results of low friction manoeuvre: wheel longitudinal slips, motors and engine torque, vehicle longitudinal acceleration, driver steering angle, vehicle trajectory

On the passive vehicle, all the four wheels lose adherence with the road, and, as a consequence, the vehicle becomes unstable. Even if the driver reacts with a steering angle demand that reaches a maximum value of 60 deg, it is not sufficient to maintain the trajectory: he loses the vehicle control.

With the control activation, the wheels' rotation is maintained under a threshold. In the same way of the relative off-line test, for each control modes the limit slip value of all the wheels is calculated referring to a road friction coefficient of 0.4, thus the differences among them are due to PI controllers' coefficients.

All the three modes allow the vehicle to achieve a satisfactory longitudinal acceleration during all the manoeuvre, while maintaining its directional stability without driver steering effort: the maximum steering value is 1 deg, while the maximum lateral displacement with respect to the straight-line trajectory is less than 1 m. This behaviour is the result of the good functioning of all three control modes in general. Considering the wheels slips value, it can be noticed that on front wheels there are no differences between *Sport*, *Comfort,* and *Wet*: for *Sport* mode, the slips values are slightly decreased when the yaw-rate control activates, but the reductions are not significant. The different controllers tuning is evident on the rear axle: *Sport* throttle scaling command on engine torque is more fluctuating than *Comfort* and *Wet* ones. As a result, it can be observed that, during the acceleration, rear wheels slips have higher peak values for *Sport* mode than for *Comfort* and *Wet* ones. This aspect influences vehicle acceleration performance: in *Comfort* and *Wet* modes, the rear wheels instantaneously acquire grip with the road, and the vehicle shows overall better traction than in *Sport*

mode.

For this manoeuvre scenario, it can be affirmed that the on-line test confirms the result of the off-line simulation.

6.2 Driver feedback

One of the advantages of the driving simulator tests is collecting the professional driver feedback about the vehicle's dynamic behaviour during the manoeuvres' performance. In this way, it is possible to change rapidly vehicle model parameters and/or, for this specific case, PI controllers' coefficients in order to reach the desired target. This process would not be easy and fast with road testing, because it involves physical components' changes and software's updates. Different configurations can be tested with a driving simulator, and the driver's feelings can be taken into account while evaluating the best solution.

For this study, it is important to know driver's feedback about how the control activation changes the vehicle response to his acceleration command. For both the test manoeuvres, in general the presence of the traction control helped the driver maintain the trajectory without a great steering effort. While repeating the acceleration on mu-split or low friction surface, in some cases it was necessary to apply a high steering angle value to complete the manoeuvre. However, the lateral displacement of the vehicle was not negligible: in a real driving situation, it would correspond to a change of roadway, which can be dangerous if considering a normal traffic condition. In the other cases, the driver lost the vehicle control because his reaction wasn't quick enough. As a consequence, the active vehicle makes him feel more comfortable and safer while performing the manoeuvre.

On the other hand, the three modes' differences are not so evident from the driver's point of view. In particular, the driver perception is that *Comfort* and *Wet* modes decrease the powertrain torques in a stabler way than *Sport* mode: especially on the rear axle, the torque is reduced instantaneously and without fluctuation, which gives the impression of a more "linear" recovery of vehicle

traction during the acceleration. *Comfort* and *Wet* modes, instead, result indistinguishable.

These considerations represent the starting point of further development of the control logic: an improvement of PI controllers' coefficients tuning can be made. Regarding *Sport* mode, in driver's opinion, the control action has to be much less reactive: consequently, the coefficients are decreased gradually until reaching a good compromise between the sufficient vehicle stability and the real driver sporty driving feel. The second objective is to differentiate more *Wet* and *Comfort* modes: the first one is made more reactive, increasing the PI coefficients value until the controller shows an unstable behaviour; for the second one, the opposite coefficient change process is made in order to obtain a sufficient difference in driver control perception. The final results are reported in Table 8.

Electric Motors		
Controller's coefficient	**Off-line value**	**On-line value**
Comfort P coefficient	8000	2000
Comfort I coefficient	3000	1000
Wet P coefficient	10000	10000
Wet I coefficient	5000	10000
Sport P coefficient	5000	10
Sport I coefficient	1000	10
Sport Yaw-rate P coefficient	80	50
Sport Yaw-rate I coefficient	90	90
Engine		
Controller's coefficient	**Off-line value**	**On-line value**
Comfort P coefficient	8	2.5
Comfort I coefficient	70	5.5
Wet P coefficient	10	12
Wet I coefficient	100	100
Sport P coefficient	6	1.3
Sport I coefficient	30	0.1

Table 8: Controllers' coefficient before and after on-line tests

7 Conclusions

In this thesis, a Traction Control System algorithm for an All-Wheel-Drive hybrid vehicle is developed. In particular, the control is applied to a high-performance vehicle whose dynamic behaviour can be adapted setting three different driving modes: *Comfort*, *Wet,* and *Sport*. The control acts on the vehicle powertrain, reducing the tractive torque when the driving wheels rotate excessively. Each of the two front wheels is connected to the corresponding onboard electric motor; hence the torque control is activated independently on the single spinning wheel. On the rear axle, both of the wheels are moved by a thermal engine whose torque is distributed by an LSD differential: depending on the control mode, when one or both the wheels exceed the slip limit value, the engine output torque is reduced closing the throttle valve. The effectiveness of the control activation is assessed through full-throttle straight-line acceleration manoeuvres, performed with off-line tests, on *VI-CarRealTime* and *MATLAB-Simulink* software, and on-line ones, on a dynamic driving simulator.

Analysing test results, it can be observed that the control improves the vehicle stability: as regards off-line tests, the driving torque reduction prevents the wheels from spinning and allows the driver to reduce the steering effort necessary to maintain the straight-line trajectory. The maximum steering angle value decreases from *Sport* to *Comfort* and *Wet* modes: this result confirms that the last two ones are more focused on vehicle safety. In general, on the active vehicle the wheels' longitudinal slips show low values; hence the vehicle itself always maintains the grip with the road and achieves a higher maximum longitudinal acceleration. The acceleration performance is enhanced in *Sport* mode, especially when some of the vehicle wheels are on a dry surface: it can be noticed for the mu-split test that the overall $a_x$value is higher for this mode; on the contrary, for a low-friction surface (wet road) the most indicated mode is the *Wet* one, because of its fastest controllers' response.

Similar conclusions can be made considering the driving simulator tests: when

the driver accelerates with the passive vehicle, it is difficult for him to maintain the vehicle control on a low-friction or a mu-split road; with the presence of the control, he feels more comfortable while performing the manoeuvre, verifying off-line simulations results. During the on-line tests, the differences among the three modes result not as evident as for the off-line simulations: the vehicle dynamic behaviour's perception is substantially the same when changing from *Sport* to *Comfort* or *Wet* mode. Starting from this feedback, a further PI controllers' tuning process is made: the tests manoeuvres are repeated several times and the controllers' coefficients are gradually modified in order to differentiate more the three modes from the driver point of view, always taking into account the target of each of them described in Paragraph 4.2.

As a conclusion, thanks to DiM tests and the opportunity to know the professional driver's feedback, the final tuning results in a robust, stable and effective Traction Control System logic.

7.1 Future developments

For this study, the control logic is designed considering that all the inputs parameters are known: during off-line tests, all the variables values are provided by the *VI-CarRealTime* vehicle model; during the on-line ones, the same model is installed on the driving simulator, which represents a full-sensorized vehicle; hence all the necessary control input channels are available. This condition is not satisfied when the control is implemented on a real vehicle; thus, the next steps for the development of the proposed control regard the deepening of this aspect. Examples of possible future studies are reported as follows:

1. The two most important control inputs from the vehicle model are the wheels' vertical loads and the tire/road friction coefficient; both generally cannot be directly measured but estimated.

   As regards the wheels' normal loads, normally the vehicles are not equipped with force transducers; hence they have to be evaluated. This is not an easy task because many factors, such as the change of vehicle mass, the load

transfers and the road conditions, affect their value. In [37] an algorithm for the wheel vertical forces estimation is proposed, which can be applied on vehicles instrumented with standard sensors.

Different methods and algorithms have been studied to estimate the road friction coefficient. In [38] the most used approaches are described: they are substantially divided into *model-based* and *experiment-based* methods. The first ones evaluate the road friction through mathematical models related to vehicle and wheel dynamics; the second ones correlate the road friction value to a variable that can be measured with sensors (acoustic, optical, temperature sensors).

2. The Pacejka maps used to evaluate the target longitudinal slips are based on known tire coefficients, which correspond to a defined kind of tire. As a consequence, the algorithm considers the tire to be always the same, while they change their characteristics during the time and can be substituted. It would be useful to evaluate, in the range of tires suitable for this kind of vehicle, how the target longitudinal slip changes, considering all the other inputs constant. Finally, a set of Pacejka coefficient proper for all the possible kinds of tires can be defined.

Bibliography

[1] K. Reif, *Brakes, Brake Control and Driver Assistance Systems: Function, Regulation and Components*, ed. Springer, 2014

[2] L. Shoubo, L. Chenglin, C. Shanglou, W. Lifang, *Traction control of Hybrid Electric Vehicle*, 2009 IEEE Vehicle Power and Propulsion Conference, September 2009, pp. 1535-1540

[3] R. Rajamani, *Vehicle dynamics and control*, ed. Springer, 2006

[4] D. Song, L. Li, X. Zeng, Y. Jiang, G. Bai, N. Yang, Y. Lei, *Traction control-integrated energy management strategy for all-wheel-drive plug-in hybrid electric vehicle*, Advances in mechanical engineering, December 2017, Vol.9

[5] W. Chen, Q. Wang, H. Xiao, L. Zhao, M. Zhu, *Integrated Vehicle Dynamics and Control*, ed. John Wiley & Sons, 2016

[6] M. M. Abdelhameed, M. Abdelaziz, N. E. Elhady, A. M. Hussein, *Development of integrated brakes and engine traction control system*, 15th International Workshop on Research and Education in Mechatronics (REM), September 2014, pp. 1-5

[7] H.-Z. Li, L. Li, L. He, M.-X. Kang, J. Song, L.-Y. Yu, C. Wu, *PID plus fuzzy logic method for torque control in Traction Control System*, International journal of automotive technology, April 2012, Vol.13 (3), pp. 441-450

[8] L. Jin, M. Ling, J. Li, *Development of a new traction control system using ant colony optimization*, Advances in mechanical engineering, August 2018, Vol.10 (8), pp. 1-12

[9] T. Akiba, R. Shirato, T. Fujita, J. Tamura, *A study of Novel Traction Control Method for Electric Motor Driven Vehicle*, 2007 Power Conversion Conference - Nagoya, April 2007, pp. 699-704

[10] H. Fujimoto, J. Amada, K. Maeda, *Review of traction and braking control for electric vehicle*, 2012 IEEE Vehicle Power and Propulsion Conference, October 2012, pp. 1292-1299

[11] V. Ivanov, D. Savitski, B. Shyrokau, *A Survey of Traction Control and Antilock Braking Systems of Full Electric Vehicles with Individually*

Controlled Electric Motors, IEEE Transactions on Vehicular Technology, September 2015, Vol.64(9), pp.3878-3896

[12] S. De Pinto, C. Chatzikomis, A. Sorniotti, G. Mantriota, *Comparison of Traction Controllers for electric Vehicles with On-Board Drivetrains*, IEEE transactions on vehicular technology, August 2017, Vol.66 (8), pp. 6715-6727

[13] D. Tavernini, M. Metzler, P. Gruber, A. Sorniotti, *Explicit Nonlinear Model Predictive Control for Electric Vehicle Traction Control*, IEEE transactions on control systems technology, July 2019, Vol.27 (4), pp. 1438-1451

[14] S. Li, C. Liao, S. Chen, L. Wang, *Traction control of Hybrid electric Vehicle*, 2009 IEEE Vehicle Power and Propulsion Conference, September 2009, pp. 1535-1540

[15] K. Han, M. Choi, B. Lee, S. B. Choi, *Development of a Traction Control System Using a Special Type of Sliding Mode Controller for Hybrid 4WD Vehicles*, IEEE transactions on vehicular technology, January 2018, Vol.67 (1), pp. 264-274

[16] J. D. Setiawan, M. Safarudin, A. Singh, *Modeling, simulation and validation of 14 DOF full vehicle model*, International Conference on Instrumentation, Communication, Information Technology, and Biomedical Engineering 2009, November 2009, pp.1-6

[17] U. Kiencke, L. Nielsen, *Automotive Control System*, Springer, 2005

[18] B. Zhang, J. Zhang, J. Yi, N. Zhang, Q. Jin, E. Mucchi, *Modal and Dynamics Analysis of a Vehicle with Kinetic Dynamic Suspension System*, Shock and Vibration, 2016, Vol.2016, 18 pages

[19] E. P. Ping, K. Hudha, H. Jamaluddin, *Automatic Steering Control for Lanekeeping Maneuver: Outer-Loop Control Design*, International Journal of Advanced Mechatronic Systems 2(5/6), January 2010, pp. 350-368

[20] M. Velardocchia, A. Vigliani, E. Galvagno, Esercitazioni del corso di Meccanica del veicolo, a.a. 2019/20, Politecnico di Torino

[21] H. B. Pacejka, *Tyre and vehicle dynamics*, ed. Butterworth-Heinemann, 2006

[22] T. D. Gillespie, *Fundamentals of vehicle dynamics*, ed. SAE, 1992

[23] G. Genta, *Motor vehicle dynamics: modelling and simulation*, ed. World Scientific, 1997

[24] W. F. Milliken, D. L. Milliken, *Race Car Vehicle Dynamics*, ed. SAE, 1995

[25] G. Genta, L. Morello, *The Automotive Chassis – Vol. 2: System Design*, ed. Springer, 2009

[26] *VI-CarRealTime 19.0 Documentation*, VI-grade GmbH, 2019

[27] Brembo Racing*, Brake Systems 2015-2016*

[28] A. G. Ulsoy, H. Peng, M. Çakmakci, *Automotive control systems*, ed. Cambridge University Press, 2012

[29] H. Lee, M. Tomizuka, *Adaptive Vehicle Traction Control*, Institute of Transportation Studies, Research Reports, Working Papers, Proceedings from Institute of Transportation Studies, UC Berkeley, 1995

[30] K. Kidera, Y. Fukao, T. Ito, *Development of Traction Control Systems for Formula One*, Honda R&D Technical Review 2009 F1 Special (The Third Era Activities), 2009, pp. 190-200

[31] K. J. Åström, T. Hägglund, *The future of PID control*, Control Engineering Practice, 2001, Vol. 9(11), pp. 1163-1175

[32] K. Ogata, *Modern control engineering*, ed. Pearson, 2010

[33] K. J. Åström, T. Hägglund, *advanced PID control*, ed. ISA, 2006

[34] VI-Grade, Driving Simulator Brochure, 2020

[35] https://www.vi-grade.com/en/about/news/danisi-engineering-launches-advanced-vehicle-dynamics-center-_39/

[36] H. Winner, S. Hakuli, F. Lotz, C. Singer, *Handbook of Driver Assistance Systems. Basic Information, Components and Systems for Active Safety and Comfort*, ed. Springer, 2016

[37] M. Doumiati, A. Victorino, A. Charara, D. Lechner, *Lateral load transfer and normal forces estimation for vehicle safety: experimental test*, Vehicle System Dynamics, 2009, Vol.47 (12), p.1511-1533

[38] S. Khaleghian, A. Emami, S. Taheri, *A technical survey on tire-road friction estimation*, Beijing: Springer Science and Business Media LLC Friction, 2017, Vol.5 (2), pp.123-146